AChE species. ColQ carries three domains: (1) an N-terminal proline-rich attachment domain that organizes the catalytic AChE subunits into a tetramer, (2) a collagen domain that forms a triple helix and contains heparin-binding domains, and (3) a C-terminal domain (CTD) enriched in charged residues and cysteines.

In previous studies, *COLQ* mutations were divided into- four classes according to their positions in ColQ and their effects on the expression of AChE species in COS cells: (1) N-terminal mutations that prevent association of $AChE_T$ with ColQ, (2) truncation mutations in the collagen domain that prevent the formation of ColQ-tailed AChE, (3) CTD missense mutations that prevent triple helical formation of ColQ, and (4) CTD mutations that do not abolish formation of ColQ-tailed AChE but affect anchoring of ColQ at the NMJ [Ohno et al., 2000]. We previously reported that p.Asp342Glu, p.Arg410Pro, and p.Arg410Glu, but not p.Cys444Tyr, at the CTD of ColQ compromise anchoring ColQ-tailed AChE to heterologous frog muscle sections [Kimbell et al., 2004]. We, however, did not show how the mutations affect anchoring of ColQ to the synaptic basal lamina. We also failed to prove pathogenicity of p.Cys444Tyr in the heterologous anchoring experiment. Two binding partners for anchoring ColQ-tailed AChE at the synaptic basal lamina have been reported to date: (1) the heparan sulfate proteoglycans such as perlecan, which bind to two heparan sulfate proteoglycan binding domains in the ColQ collagen domain [Arikawa-Hirasawa et al., 2002], and (2) the extracellular domain of MuSK, a muscle-specific receptor tyrosine kinase, on the postsynaptic membrane, which binds to the CTD of ColQ [Cartaud et al., 2004]. We recently demonstrated that anti-MuSK autoantibodies in patients with myasthenia gravis block binding of ColQ to MuSK [Kawakami et al., 2011]. We also reported that intravenous or intramuscular administration of adeno-associated virus serotype 8 (AAV8) carrying human *COLQ* efficiently anchors ColQ-tailed AChE at the NMJ [Ito et al., 2012]. We proved that ColQ-tailed AChE moves from one muscle to another and anchors to the synaptic basal lamina by exploiting the proprietary binding affinity for synaptic basal lamina, which we named the protein-anchoring therapy.

We here report three patients with AChE deficiency harboring *COLQ* mutations in the collagen domain and CTD. We examined the effects of the CTD mutations on interaction between ColQ and MuSK by in vitro and in vivo assays and found that the CTD mutations impair this interaction.

Materials and Methods

Patients

All human studies were performed under approvals of the institutional review boards of Nagoya University Graduate School of Medicine, National Center of Neurology and Psychiatry, Juntendo University Faculty of Medicine, and Utano National Hospital. Three patients participated in the study after appropriate informed consents were given. A mutation analysis had been done when they were 7, 12, and 19 years of age, respectively. All had respiratory distress or poor sucking at birth, slight delay in walking, fatigability since early childhood, normal intelligence, no anti-AChR and anti-MuSK antibodies, a decremental electromyographic response, repetitive CMAP to a single nerve stimulus, and no response to anticholinesterase medications (Table 1).

Mutation Analysis

Genomic DNA was isolated from blood with QIAamp Blood Mini Kit (Qiagen, Hilden, Germany). Poor response to anticholinesterases suggested endplate AChE deficiency and slow channel syndrome. We thus directly sequenced 17 constitutive *COLQ* exons and their flanking regions with CEQ8000 sequencer (Beckman Coulter, Brea, CA). Names of all mutations were checked using Mutalyzer (http://www.lovd.nl/mutalyzer/). Identified mutations were submitted to an LSDB for the *COLQ* gene (http://www.lovd.nl/COLQ). As mutations were identified in *COLQ* in all the patients, we did not go into sequencing of *CHRNA1* (NM_00079.3; MIM #100690), *CHRNB1* (NM_009601.4; MIM #100710), *CHRND* (NM_021600.2; MIM #100720), and *CHRNE* (NM_000080.3; MIM #100725) encoding the AChR α, β, δ, and ε subunits, respectively.

Construction of Expression Vectors

Human $ACHE_T$, *COLQ* cDNAs, and LacZ were cloned and introduced into a cytomegalovirus-based mammalian expression vector pTargeT (Promega, Madison, WI) [Ohno et al., 1998]. Each mutation was introduced into *COLQ* cDNA using the QuikChange site-directed mutagenesis kit (Stratagene). The extracellular domain (aa 1–393) of human *MUSK* (NM_001166280.1; MIM #601296) cDNA (Open Biosystems/Thermo Scientific, Waltham, MA) was cloned into a mammalian expression vector pAPtag-5 (GenHunter, Nashville, TN) at the *Nbe*I and *Xbo*I sites upstream of a myc epitope [Kawakami et al., 2011].

Transfection and AChE Extraction

Wild-type or mutant pTargeT-*COLQ* was transfected into COS7 cells along with pTargeT-$ACHE_T$ in a 10-cm dish using X-tremeGENE 9 DNA Transfection Reagent (Roche Diagnostics, Indianapolis, IN). Cells were incubated at 37°C for 48 hr and scraped from dish in Tris–HCl buffer (50 mM Tris–HCl [pH 7.0], 0.5% Triton X-100, 0.2 mM EDTA, 2 μg/ml leupeptin, 1 μg/ml pepstatin, and 0.1 μmol/ml benzamidine) containing 1 M NaCl. The extract was vortexed in a 1.5-ml tube and centrifuged at 14,000*g* for 5 min, and the supernatant was obtained.

Sedimentation Analysis

A sedimentation analysis was performed as previously described [Ohno et al., 1998]. The AChE-containing supernatant was applied on a 5%–20% sucrose density gradient, which was made in Tris–HCl buffer along with β-galactosidase (16.1 S) and alkaline phosphatase (6.1 S) as internal sedimentation standards. Centrifugation was performed in a Beckman SW41Ti rotor at 4°C for 21 hr at 178300*g*. The collected fractions were assayed for AChE activities using the Ellman method [Ellman et al., 1961] and determined the absorbance at 420 nm using a Sunrise Absorbance Reader (Tecan, Männedorf, Switzerland).

Isolation of ColQ-Tailed AChE on a Heparin–Agarose Column

For isolation of ColQ-tailed AChE, the extract was diluted in Tris–HCl buffer containing 0.2 M NaCl and loaded onto a HiTrap Heparin HP column (GE Healthcare, Buckinghamshire, UK). We washed the column with five volumes of Tris–HCl buffer containing 0.2 M NaCl, and eluted ColQ-tailed AChE with Tris–HCl buffer containing 1 M NaCl. We concentrated the eluate with an Amicon Ultra-4 Centrifugal Filter (50K) (Millipore, Billerica, MA) [Kawakami et al., 2011; Kimbell et al., 2004].

Table 1. Clinical Features and Mutations

Pt.	Sex	Age	Onset	Walking	Noc. NIV	Edrophonium i.v.	RNS	rCMAP	Exon	Nucleotide change	Amino-acid change
1	M	19 y	Birth	19 m	12 y	No change	-52%	+	11	c.679C>T	p.Arg227X
									14	c.965T>A	p.Val322Asp
2	M	12 y	Birth	24 m	11 y	Respiratory distress	-32%	+	17	c.1339G>C[a]	p.Asp447His[a]
3	M	7 y	3 y	18 m	Not used	Improved	-79%	+	17	c.1331G>A	p.Cys444Tyr
									17	c.1354C>T	p.Arg452Cys

[a]Homozygous mutation.
Exon numbers are according to GenBank Accession NM_005677.3. Mutations are numbered according to NM_005677.3 (cDNA) and NP_005668.2 (protein). cDNA number +1 corresponds to the A of the ATG translation initiation codon.
Pt., patient; Noc. NIV, nocturnal noninvasive ventilation; RNS, repetitive nerve stimulation at 3 Hz of ulnar or accessory nerves; rCMAP, repetitive compound muscle action potential; m, months; y, years.

Transplantation of ColQ-tailed AChE to NMJs of *Colq*$^{-/-}$ Mice

We obtained approvals of the *Colq*$^{-/-}$ mice[Feng et al., 1999] studies by the Animal Care and Use Committee of the Nagoya University. We prepared 10-μm-thick sections of quadriceps muscles of *Colq*$^{-/-}$ mice with a Leica CW3050–4 cryostat at -20°C, and stored at -80°C until used. The muscle sections were fixed in acetone for 15 min. The stock solutions of ColQ-tailed AChE were diluted in Tris–HCl buffer containing 1 M NaCl and 5 mg/ml each of bovine serum albumin, chicken ovalbumin, and gelatin to give an Ellman unit equivalent to 1–2 ng of Torpedo AChE (Sigma, St. Louis, MO), and the NaCl concentration was adjusted to 0.5 M. To adjust the ionic strength of the solution, we added 50 mM Tris–HCl buffer stepwise over a period of 3 hr to 0.3 M NaCl. The slides were placed in a humidified chamber and incubated overnight at room temperature [Kimbell et al., 2004; Rotundo et al., 1997].

Immunofluorescence

For preparation of immunofluorescence, muscle sections were blocked with 5% horse serum in phosphate-buffered saline for 20 min. We detected ColQ-tailed AChE by anti-ColQ antibody [Ito et al., 2012] and anti rabbit-FITC secondary antibody at 1:100 (Vector Lab., Burlingame, CA), along with 2.5 μg/ml Alexa-594-conjugated α-bungarotoxin (Sigma) for visualizing AChR. Signals of ColQ and AChR were examined with fluorescent microscope, BX60 (Olympus, Tokyo, Japan). We analyzed more than 10 muscle sections for each experiment and representative images are indicated in the figures.

Preparation of the Extracellular Domain of MuSK

pAPtag-5 carrying hMuSKect-myc was transfected into HEK293 cells in a 10-cm dish using the calcium phosphate method. The hMuSKect-myc was purified with the c-myc-Tagged Protein Mild Purification Kit version 2 (MBL, Nagoya, Japan) [Kawakami et al., 2011].

In Vitro Plate-Binding assay for ColQ–MuSK Interaction

The Maxi-Sorp Immuno Plate (Nunc/Thermo Scientific) was coated with purified hMuSKect-myc at 4°C overnight and then blocked with phosphate-buffered saline containing 1% bovine serum albumin at room temperature for 1 hr. We incubated an equal Ellman unit of wild-type or mutant ColQ-tailed AChE at 4°C for 4 hr and then quantified the bound ColQ-tailed AChE by the Ellman method. Each time before we moved to the next step, we washed the plate three times with phosphate-buffered saline [Kawakami et al., 2011].

In Vivo Electroporation of pTarget-*COLQ*

The tibialis anterior muscles of *Colq*$^{-/-}$ mice were injected with 50 μg each of pTargeT-*COLQ* and pTargeT-LacZ plasmids. In vivo transfection was performed using an in vivo electroporator (CUY21EDIT; BEX Co., Ltd., Tokyo, Japan). A pair of electrode needles was inserted into the muscle in the longitudinal direction to a depth of 4 mm to encompass the plasmid-injected site. Pulses of 50 V and 25-msec were administered every 1 sec three times in forward polarity and three more times in the opposite polarity [Aihara and Miyazaki, 1998]. Seven days after the electroporation, mice were sacrificed and tibialis anterior muscles were analyzed.

AAV8-Mediated Expression of Mutant ColQ in *Colq*$^{-/-}$ Mice

We prepared wild-type and mutant pAAV8-*COLQ* and intravenously administered them to *Colq*$^{-/-}$ mice as described previously [Ito et al., 2012]. We inserted the wild-type human *COLQ* or mutant human *COLQ* harboring p.Asp447His into downstream of a CMV promoter in the pAAV-MCS vector using the AAV Helper-Free system (Stratagene). We employed AAV serotype 8 that can efficiently infect skeletal muscles. We injected 2×10^{12} vector genomes of wild-type or mutant pAAV-*COLQ* to the tail vein of 4-week-old male *Colq*$^{-/-}$ mice. Similar copies of wild-type pAAV8-*COLQ* and mutant pAAV8-*COLQ*-p.Asp447His genomes were transduced into muscle cells with a mean ratio of 1.07 (mutant transgene/wild-type transgene, $n = 3$). We quantified motor functions up to 4 weeks after injection. Muscle weakness and fatigability were measured with a rotarod apparatus (Ugo Basile). Mice were allowed to take a rest for 1 hr between each rotarod task and an average of three measurements was taken. Spontaneous running-wheel activities were used to quantify voluntary exercises. Each mouse was placed in a standard cage equipped with a counter-equipped running wheel (diameter, 14.7 cm; width, 5.2 cm; Ohara Medical Corp., Tokyo, Japan). The running distances were recorded every 24 hr. At 6 weeks after injection, mice were sacrificed and sections of skeletal muscles were stained for AChR and ColQ to visualize the transduced ColQ-tailed AChE as described above.

Results

Mutation Analysis

On the basis of combined clinical and electrophysiological features such as early age of onset, negative response to cholinesterase inhibitors, respiratory insufficiency, and repetitive muscle response [Abicht et al., 2012; Engel, 2012], we first sequenced *COLQ* and identified that each patient carried two mutant *COLQ* alleles. Patient 1 had heterozygous [c.679C>T, p.Arg227X] +

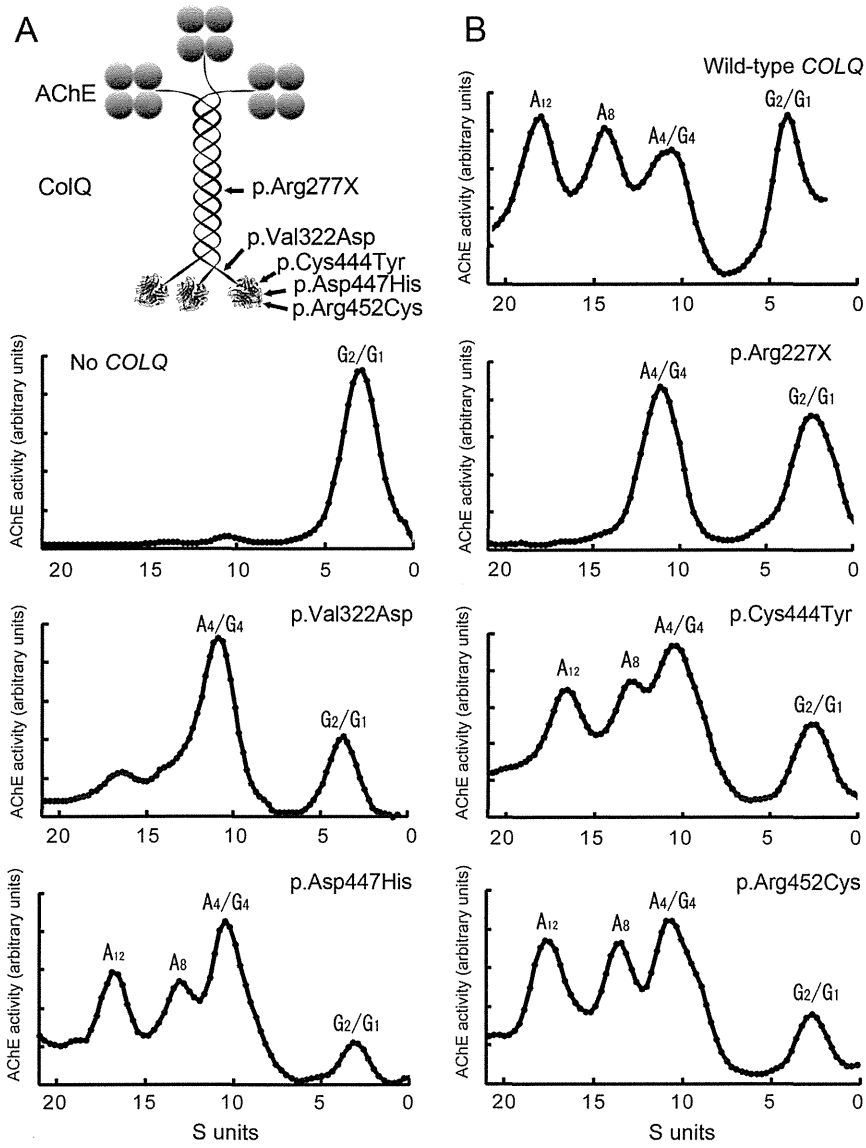

Figure 1. **A:** Schematic presentation of positions of the identified mutations in ColQ. **B:** Sedimentation profiles of AChE species extracted from COS cells transfected with wild-type *ACHE*$_T$ cDNA and indicated *COLQ* cDNA. p.Arg227X is in the collagen domain, the other four missense mutations are in the C-terminal domain. p.Val322Asp has a small ~16-S peak (A_{12} species), whereas the other missense mutations in the C-terminal region do not abolish formation of asymmetric AChE species. G_1, G_2, and G_4, globular forms; A_4, A_8, and A_{12}, asymmetric forms.

[c.965T>A, p.Val322Asp] mutations. Patient 2 was heterozygous for [c.1331G>A, p.Cys444Tyr] + [c.1354C>T, p.Arg452 Cys]. Patient 3 had a homozygous [c.1339G>C, p.Asp447His] mutation (Fig. 1A, Table 1, Supp. Fig. S1). We traced the mutations in the parents of patients 1 and 3, and found that the mutation on each allele was inherited from unaffected parents. In patient 2, we confirmed heterozygosity by cloning each allele of exon 17 and sequenced them. Among the five mutations, only c.1331G>A, p.Cys444Tyr was previously identified in another Japanese patient [Ohno et al., 2000], but its pathogenicity remained elusive [Kimbell et al., 2004]. The other four mutations were novel. All the amino acids at mutated codons were conserved across species [Ohno et al., 1998].

Sedimentation Profiles of Mutations

Four missense mutations were in CTD and the nonsense p.Arg227X was in the collagen domain. We first examined the effects of the mutations on formation of asymmetric ColQ-tailed AChE species in COS cells. The p.Arg227X mutation that truncates ColQ in its collagen domain did not produce normal A_{12} species of ColQ-tailed AChE, as has been observed in other truncation mutations in the collagen domain [Ohno et al., 1998; 2000]. The p.Val322Asp mutation close to the N-terminal end of CTD similarly failed to produce A_{12} species. By contrast, the other three CTD mutations (p.Cys444Tyr, p.Asp447His, and p.Arg452Cys) produced

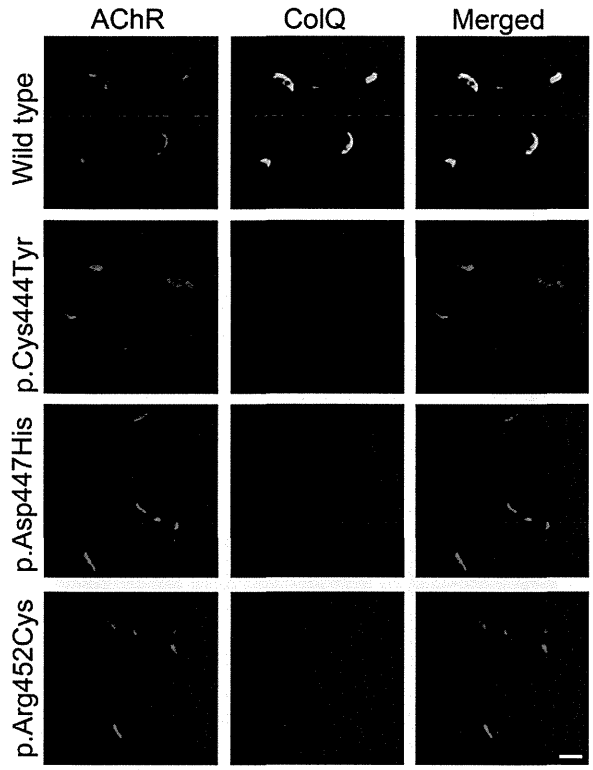

Figure 2. In vitro overlay assays. Plasmid encoding the indicated CTD mutations of human ColQ were cotransfected into COS cells together with a plasmid encoding the wild-type human $AChE_T$ catalytic subunit. The A_{12} AChE expressed in COS cells was isolated and overlaid on a 10-μm quadriceps muscle section of *Colq*$^{-/-}$ mice. ColQ-tailed AChE molecules harboring the indicated mutations do not colocalize with AChRs. ColQ is stained with anti-ColQ antibody and AChR with Alexa594-labeled α-bungarotoxin. Scale bar = 20 μm.

normal or slightly reduced peaks of asymmetric A_4, A_8, and A_{12} species compared to the wild-type (Fig. 1B).

Overlay of CTD Mutants to the NMJ of *Colq*$^{-/-}$ Mice

We overlaid the purified recombinant human ColQ-tailed AChE protein complex on a section of skeletal muscle of *Colq*$^{-/-}$ mice. Wild-type ColQ-tailed AChE colocalized with AChR at the NMJs, whereas ColQ-tailed AChE with p.Cys444Tyr, p.Asp447His, and p.Arg452Cys mutations failed to colocalize with AChR (Fig. 2). This assay showed that these CTD mutations impair anchoring of ColQ at the vertebrate NMJs.

In Vitro Plate-Binding Assay for ColQ–MuSK Interaction

As the synaptic anchorage of AChE by ColQ is partly dependent on the association of ColQ with MuSK [Cartaud et al., 2004], we next examined whether the CTD mutations had an effect on the interaction of human ColQ and human MuSK using an in vitro plate-binding assay. We coated the plate with purified hMuSKect-myc, and added a fixed amount of the purified recombinant human ColQ-tailed AChE protein complex. The bound AChE was quantified by the Ellman method. AChE activities of the CTD mutants carrying p.Cys444Tyr, p.Asp447His, and p.Arg452Cys were significantly lower than that of wild-type CTD (Fig. 3). These results showed that impaired anchoring of the mutant ColQ-tailed AChE was due to the lack of interaction between ColQ and MuSK.

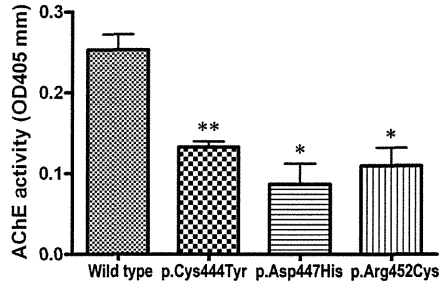

Figure 3. In vitro plate-binding assays. The extracellular domain of human MuSK (hMuSKect-myc) was coated on a 96-well plate. Purified recombinant ColQ-tailed AChE was overlaid on the plate. Bound ColQ-tailed AChE was quantified by AChE activity. $^*P < 0.05$, $^{**}P < 0.01$ by Student's *t*-test.

In Vivo Electroporation of *COLQ* with CTD Mutations into the Muscles of *Colq*$^{-/-}$ Mice

To confirm whether the three CTD mutants indeed impair anchoring of ColQ-tailed AChE to the NMJ in vivo, we electroporated wild-type and mutant pTargeT-*COLQ* constructs to tibialis anterior muscles of *Colq*$^{-/-}$ mice. We first confirmed that the pTargeT-LacZ plasmid is efficiently transduced into muscle fibers (Fig. 4A). ColQ-tailed AChE harboring p.Cys444Tyr, p.Asp447His, and p.Arg452Cys in CTD did not anchor to the NMJs of *Colq*$^{-/-}$ mice (Fig. 4), although real-time RT-PCR revealed similar expression levels of the wild-type and mutant *COLQ* mRNAs (ranges of *COLQ*/*Gapdh* mRNAs = 0.03 to 0.11 for wild-type and three mutants). These studies revealed that the three mutant ColQ molecules were incompetent for anchoring to the NMJ in vivo.

AAV8-Mediated Expression of Mutant ColQ in *Colq*$^{-/-}$ Mice

We previously reported the protein-anchoring therapy for *Colq*$^{-/-}$ mice, in which ColQ-tailed AChE is moved to and anchored to remote NMJs using its proprietary binding affinities for perlecan and MuSK [Ito et al., 2012]. To directly prove that the CTD mutations compromise anchoring of ColQ to the NMJ in a model animal, we intravenously administered wild-type and p.Asp447His-mutant AAV8-*COLQ* to *Colq*$^{-/-}$ mice, and analyzed motor functions and histological localization of ColQ. Motor functions evaluated by the dwell time on a rotarod (Fig. 5A) and by voluntary movements (Fig. 5B) were prominently improved in *Colq*$^{-/-}$ mice treated with wild-type *COLQ* but not with p.Asp447His-*COLQ*. Histological studies similarly showed that ColQ was colocalized to AChR in *Colq*$^{-/-}$ mice treated with AAV-wild-type *COLQ* but not with AAV-p.Asp447His-*COLQ* (Fig. 5C).

Discussion

CMSs have a variety of causes that lead to defects in the NMJ signal transmission. Elucidation of the molecular pathomechanisms is essential to develop and provide a specific treatment for CMS patients. Ephedrine and albuterol are effective for patients with

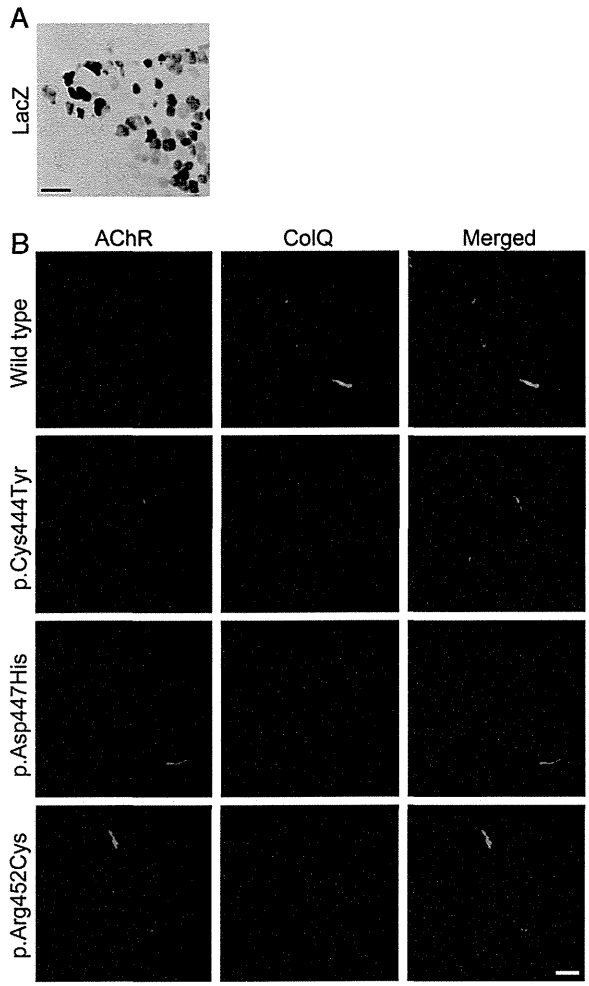

Figure 4. In vivo electroporation. **A:** Histochemical staining for β-galactosidase activity in the muscle after gene transfer of pTargeT-lacZ with electroporation. The transverse section of the muscle was stained with X-gal. **B:** Immunocytochemistry using serial muscle sections showed that ColQ-tailed AChE molecules harboring p.Val322Asp, p.Asp447His, p.Cys444Tyr, and p.Arg452Cys in ColQ, do not colocalize with AChRs in tibialis anterior muscles of *Colq*$^{-/-}$ mice. ColQ is stained with anti-ColQ antibody and AChR with Alexa594-labeled α-bungarotoxin. Scale bar = 100 μm (**A**) and 20 μm (**B**).

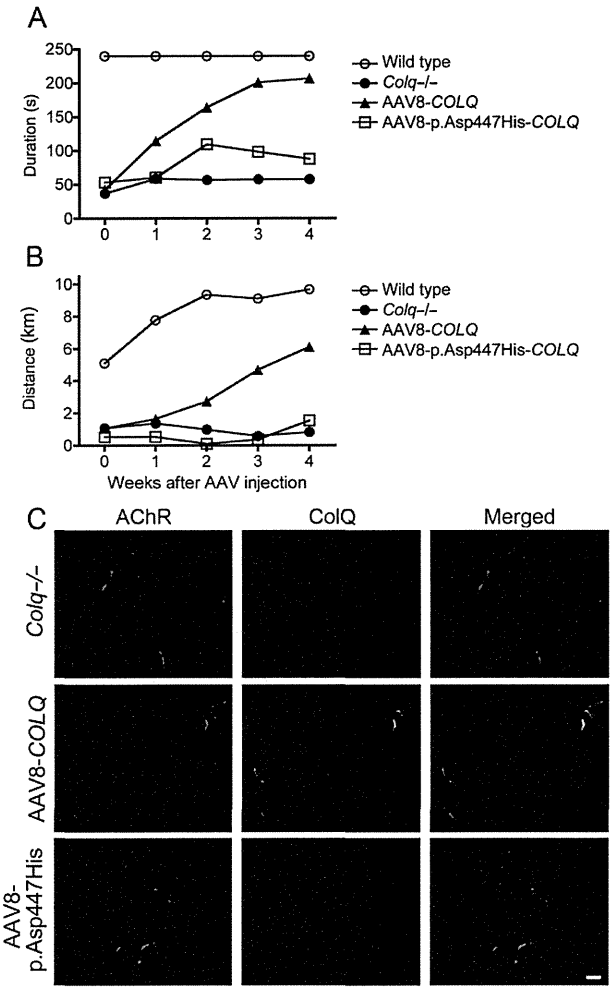

Figure 5. AAV8-mediated expression of mutant ColQ in *Colq*$^{-/-}$ mice. **A**: Temporal profiles of dwell times on a rotarod that linearly accelerated from 0 to 40 rpm in 240 sec. **B**: Voluntary movements per day were quantified with a counter-equipped running wheel. **C**: Visualization of ColQ-AChE and AChR on the section of skeletal muscle using anti-ColQ antibody and α-bungarotoxin, respectively. AAV8-*COLQ*-p.Asp447His failed to anchor ColQ-tailed AChE to the NMJ. Scale bar = 20 μm.

endplate AChE deficiency harboring *COLQ* mutations [Chan et al., 2012; Engel et al., 2010]. Cholinesterase inhibitors cannot improve neuromuscular transmission and often worsen myasthenic symptoms and respiratory conditions. Therefore, an early genetic diagnosis is important for the patients. Clinical features of the three patients prompted us to search for mutations in *COLQ*, and indeed we detected five *COLQ* mutations. Four of them are novel and p.Cys444Tyr has been previously reported in another Japanese patient [Ohno et al., 2000]. It is interesting to note that the five mutations are unique to Japanese patients, which suggests that all the mutations have recently arisen in the patients' families and are unlikely to be founder mutations.

In 1998, we cloned human *COLQ* cDNA, identified its genomic structure, and detected *COLQ* mutations in patients with endplate AChE deficiency [Ohno et al., 1998]. We also proved that mutations in the collagen domain impair formation of ColQ-tailed AChE [Ohno et al., 1998]. We later reported four classes of *COLQ* mutations as stated in the introduction, and proved pathogenicity in three classes but not in a class comprising CTD mutations [Ohno et al., 1999; 2000]. We next proved pathogenicity of five mutations (p.Arg315X, p.Asp342Glu, p.Gln371X, p.Arg410Gln, and p.Arg410Pro) in CTD using the heterologous overlay of human ColQ-tailed AChE to the frog muscles, but another mutation, p.Cys444Tyr, had no effect on anchoring of ColQ to the frog NMJ [Kimbell et al., 2004]. To summarize, we have reported 23 *COLQ* mutations and have succeeded in proving the pathogenicity in 22 mutations [Kimbell et al., 2004; Ohno et al., 1998; 1999; 2000; Shapira et al., 2002]. p.Cys444Tyr in CTD has thus been the only mutation that we failed to prove why the patient was deficient for AChE. Donger et al. (1998) reported p.Tyr430Ser in CTD in a patient with endplate AChE deficiency, but the sedimentation analysis yielded normal asymmetric species of AChE. The p.Tyr430Ser mutation was later employed to prove that CTD binds to MuSK by immunoprecipitation experiments [Cartaud et al., 2004]. Four

additional mutations (p.Arg341Gly, p.Cys386Ser, p.Cys417Tyr, and p.Thr441Ala) in CTD have been reported by others but none have been functionally analyzed [Mihaylova et al., 2008; Muller et al., 2004].

In the present study, we found four missense mutations (p.Val322Asp, p.Asp447His, p.Cys444Tyr, and p.Arg452Cys) in CTD and one truncation mutation (p.Arg227X) in the collagen domain in three patients with endplate AChE deficiency. Three mutations (p.Val322Asp, p.Asp447His, and p.Arg452Cys) in CTD have not been functionally characterized and one was p.Cys444Tyr, for which the pathogenicity remained elusive. We characterized the functional consequences of these mutations.

The analysis of sedimentation profiles revealed that p.Arg227X and p.Val322Asp abolish formation of normal asymmetric A_{12} species of AChE. p.Val322Asp is the only mutation that affects formation of A_{12} and is the only mutation that introduces a negatively charged residue in CTD. We previously reported that 1082delC in CTD introduces 64 hydrophobic missense residues after the frameshift, which prevents triple helix formation [Ohno et al., 2000]. CTD is enriched with prolines, cysteines, and charged residues. The hydrophobicity profile is likely to be essential in CTD. p.Val322Asp introduces a hydrophilic aspartate residue, and disrupts a hydrophobic cluster close to the N-terminal end of CTD (Supp. Fig. S2A). Prediction of a secondary structure similarly demonstrates shortening of a β-sheet and de novo insertion of a turn before an α-helix (Supp. Fig. S2B). We do not observe these gross alterations in predicted structures with p.Cys444Tyr, p.Asp447His, and p.Arg452Cys (Supp. Fig. S2). p.Val322Asp is thus likely to compromise the tertiary structure of CTD and leads to defective triple helix formation.

The analysis of sedimentation profiles showed that the other CTD mutations, p.Cys444Tyr, p.Asp447His, and p.Arg452Cys, generated normal asymmetric A_{12} species of AChE. We next examined the anchoring competence of these mutations. We had previously employed frog muscles to analyze anchoring incompetence of CTD mutations, but failed to prove it for p.Cys444Tyr [Kimbell et al., 2004]. We thus used the vertebrate NMJs of *Colq*$^{-/-}$ mice, and proved that all three mutations are not able to anchor to the mouse NMJ. Anchoring competence of p.Cys444Tyr to frog NMJs but not to mouse NMJs suggests that p.Cys444Tyr does not grossly change the conformation of CTD and is likely to be a mild mutation. Indeed, the onset of patient 3 carrying p.Cys444Tyr was at the age of 3 years, and the patient started walking at 18 months, which are the mildest among the three currently analyzed patients.

To further dissect the underlying molecular bases of anchoring incompetence of p.Cys444Tyr, p.Asp447His, and p.Arg452Cys, we quantified the ColQ–MuSK interaction by the in vitro plate-binding assay, which enabled us to estimate the binding affinities of these two molecules. The three missense mutations decreased the activities of ColQ-tailed AChE bound to MuSK to ~50% or less, which suggests that ~50% reduction of the binding affinity is likely to be required to compromise anchoring of ColQ to the NMJ.

Moreover, we demonstrated the pathogenicity of the mutations in a model animal for the first time. We electroporated the three CTD mutations into tibialis anterior muscles of *Colq*$^{-/-}$ mice, and found that each mutation was indeed anchoring-incompetent. To further prove the pathogenicity of one of the mutations in *Colq*$^{-/-}$ mice, we intravenously injected AAV8-*COLQ*-p.Asp447His to *Colq*$^{-/-}$ mice and found that motor deficits remained essentially the same and anchoring of ColQ was not observed at the NMJs.

In vitro plate-binding assays revealed ~50% reduction of binding affinity of ColQ for MuSK for p.Cys444Tyr, p.Asp447His, and p.Arg452Cys (Fig. 3), but these mutants were not at all anchored to the NMJ by in vitro overlay assay (Fig. 2), in vivo electroporation (Fig. 4), and AAV8 treatment (Fig. 5). Among the three mutants, p.Cys444Tyr showed the most preserved binding affinity for MuSK, which, however, was not sufficient to anchor the mutant ColQ to the NMJ in in vitro overlay assay (Fig. 2) and in vivo electroporation (Fig. 4). The presence of heparan sulfate proteoglycans like perlecan at the NMJ in these assays was unlikely to sufficiently compensate for the defective CTD-MuSK interaction, which also underscores a pivotal role of CTD-MuSK interaction on binding of ColQ to the NMJ. Although the same amount of ColQ-tailed AChE was used for in vitro plate-binding and in vitro overlay assays, the amount of MuSK (>150 ng/well) used in in vitro plate-binding assay was likely to be much more than that at the NMJ in in vitro overlay assay, which may account for the difference in up to 50% preservation of ColQ binding in in vitro plate-binding assay and complete lack of ColQ binding in in vitro overlay assay.

Acknowledgments

We thank Yasutaka Ohya, Kumiko Yano, and Koji Nomaru at Division for Research of Laboratory Animals of Nagoya University for technical assistance.

Disclosure statement: The authors declare no conflict of interest.

References

Abicht A, Dusl M, Gallenmuller C, Guergueltcheva V, Schara U, Della Marina A, Wibbeler E, Almaras S, Mihaylova V, von der Hagen M, Huebner A, Chaouch A, et al. 2012. Congenital myasthenic syndromes: achievements and limitations of phenotype-guided gene-after-gene sequencing in diagnostic practice: a study of 680 patients. Hum Mutat 33:1474–1484.

Aihara H, Miyazaki J. 1998. Gene transfer into muscle by electroporation in vivo. Nat Biotechnol 16:867–870.

Arikawa-Hirasawa E, Rossi SG, Rotundo RL, Yamada Y. 2002. Absence of acetylcholinesterase at the neuromuscular junctions of perlecan-null mice. Nat Neurosci 5:119–123.

Cartaud A, Strochlic L, Guerra M, Blanchard B, Lambergeon M, Krejci E, Cartaud J, Legay C. 2004. MuSK is required for anchoring acetylcholinesterase at the neuromuscular junction. J Cell Biol 165:505–515.

Chan SH, Wong VC, Engel AG. 2012. Neuromuscular junction acetylcholinesterase deficiency responsive to albuterol. Pediatr Neurol 47:137–140.

Donger C, Krejci E, Pou Serradell A, Eymard B, Bon S, Nicole S, Chateau D, Gary F, Fardeau M, J. M, Guicheney P. 1998. Mutation in the human acetylcholinesterase-associated collagen gene, *COLQ*, is responsible for congenital myasthenic syndrome with end-plate acetylcholinesterase deficiency (Type Ic). Am J Hum Genet 63:967–975.

Ellman GL, Courtney KD, Andres V, Jr., Feather-Stone RM. 1961. A new and rapid colorimetric determination of acetylcholinesterase activity. Biochem Pharmacol 7:88–95.

Engel AG. 2012. Congenital myasthenic syndromes in 2012. Curr Neurol Neurosci Rep 12:92–101.

Engel AG, Lambert EH, Gomez MR. 1977. A new myasthenic syndrome with end-plate acetylcholinesterase deficiency, small nerve terminals, and reduced acetylcholine release. Ann Neurol 1:315–330.

Engel AG, Ohno K, Sine SM. 2003. Sleuthing molecular targets for neurological diseases at the neuromuscular junction. Nat Rev Neurosci 4:339–352.

Engel AG, Shen XM, Selcen D, Sine SM. 2010. What have we learned from the congenital myasthenic syndromes. J Mol Neurosci 40:143–153.

Feng G, Krejci E, Molgo J, Cunningham JM, Massoulie J, Sanes JR. 1999. Genetic analysis of collagen Q: roles in acetylcholinesterase and butyrylcholinesterase assembly and in synaptic structure and function. J Cell Biol 144:1349–1360.

Ito M, Suzuki Y, Okada T, Fukudome T, Yoshimura T, Masuda A, Takeda S, Krejci E, Ohno K. 2012. Protein-anchoring strategy for delivering acetylcholinesterase to the neuromuscular junction. Mol Ther 20:1384–1392.

Kawakami Y, Ito M, Hirayama M, Sahashi K, Ohkawara B, Masuda A, Nishida H, Mabuchi N, Engel AG, Ohno K. 2011. Anti-MuSK autoantibodies block binding of collagen Q to MuSK. Neurology 77:1819–1826.

Kimbell LM, Ohno K, Engel AG, Rotundo RL. 2004. C-terminal and heparin-binding domains of collagenic tail subunit are both essential for anchoring acetylcholinesterase at the synapse. J Biol Chem 279:10997–11005.

Massoulie J. 2002. The origin of the molecular diversity and functional anchoring of cholinesterases. Neurosignals 11:130–143.

Mihaylova V, Muller JS, Vilchez JJ, Salih MA, Kabiraj MM, D'Amico A, Bertini E, Wolfle J, Schreiner F, Kurlemann G, Rasic VM, Siskova D, et al. 2008. Clinical and molecular genetic findings in COLQ-mutant congenital myasthenic syndromes. Brain 131:747–759.

Muller JS, Petrova S, Kiefer R, Stucka R, Konig C, Baumeister SK, Huebner A, Lochmuller H, Abicht A. 2004. Synaptic congenital myasthenic syndrome in three patients due to a novel missense mutation (T441A) of the COLQ gene. Neuropediatrics 35:183–189.

Ohno K, Brengman J, Tsujino A, Engel AG. 1998. Human endplate acetylcholinesterase deficiency caused by mutations in the collagen-like tail subunit (ColQ) of the asymmetric enzyme. Proc Natl Acad Sci USA 95:9654–9659.

Ohno K, Brengman JM, Felice KJ, Cornblath DR, Engel AG. 1999. Congenital endplate acetylcholinesterase deficiency caused by a nonsense mutation and an A–>G splice-donor-site mutation at position +3 of the collagenlike-tail-subunit gene (COLQ): how does G at position +3 result in aberrant splicing? Am J Hum Genet 65:635–644.

Ohno K, Engel AG, Brengman JM, Shen X-M, Heidenrich FR, Vincent A, Milone M, Tan E, Demirci M, Walsh P, Nakano S, Akiguchi I. 2000. The spectrum of mutations causing endplate acetylcholinesterase deficiency. Ann Neurol 47:162–170.

Rotundo RL, Rossi SG, Anglister L. 1997. Transplantation of quail collagen-tailed acetylcholinesterase molecules onto the frog neuromuscular synapse. J Cell Biol 136:367–374.

Shapira YA, Sadeh ME, Bergtraum MP, Tsujino A, Ohno K, Shen XM, Brengman J, Edwardson S, Matoth I, Engel AG. 2002. Three novel COLQ mutations and variation of phenotypic expressivity due to G240X. Neurology 58:603–609.

Sigoillot SM, Bourgeois F, Lambergeon M, Strochlic L, Legay C. 2010. ColQ controls postsynaptic differentiation at the neuromuscular junction. J Neurosci 30:13–23.

HMG Advance Access published November 29, 2013

Human Molecular Genetics, 2013 **1–13**
doi:10.1093/hmg/ddt578

LRP4 third β-propeller domain mutations cause novel congenital myasthenia by compromising agrin-mediated MuSK signaling in a position-specific manner

Bisei Ohkawara[1], Macarena Cabrera-Serrano[3], Tomohiko Nakata[1], Margherita Milone[3], Nobuyuki Asai[1], Kenyu Ito[1], Mikako Ito[1], Akio Masuda[1], Yasutomo Ito[2], Andrew G. Engel[3,*] and Kinji Ohno[1,*]

[1]Division of Neurogenetics, Center for Neurological Diseases and Cancer and [2]Division for Medical Research Engineering, Nagoya University Graduate School of Medicine, Nagoya, Japan [3]Department of Neurology, Mayo Clinic, Rochester, MN, USA

Received June 10, 2013; Revised October 15, 2013; Accepted November 11, 2013

Congenital myasthenic syndromes (CMS) are heterogeneous disorders in which the safety margin of neuromuscular transmission is compromised by one or more specific mechanisms. Using Sanger and exome sequencing in a CMS patient, we identified two heteroallelic mutations, p.Glu1233Lys and p.Arg1277His, in *LRP4* coding for the postsynaptic low-density lipoprotein receptor-related protein 4. LRP4, expressed on the surface of the postsynaptic membrane of the neuromuscular junction, is a receptor for neurally secreted agrin, and LRP4 bound by agrin activates MuSK. Activated MuSK in concert with Dok-7 stimulates rapsyn to concentrate and anchor AChR on the postsynaptic membrane and interacts with other proteins implicated in the assembly and maintenance of the neuromuscular junction. LRP4 also functions as an inhibitor of Wnt/beta-catenin signaling. The identified mutations in *LRP4* are located at the edge of its 3rd beta-propeller domain and decrease binding affinity of LRP4 for both MuSK and agrin. Mutations in the LRP4 3rd beta-propeller domain were previously reported to impair Wnt signaling and cause bone diseases including Cenani–Lenz syndactyly syndrome and sclerosteosis-2. By analyzing naturally occurring and artificially introduced mutations in the LRP4 3rd beta-propeller domain, we show that the edge of the domain regulates the MuSK signaling whereas its central cavity governs Wnt signaling. We conclude that *LRP4* is a new CMS disease gene and that the 3rd beta propeller domain of LRP4 mediates the two signaling pathways in a position-specific manner.

INTRODUCTION

Congenital myasthenic syndromes (CMS) are diverse disorders in which the safety margin of neuromuscular transmission is compromised by deficiency or abnormal function of an endplate (EP)-associated protein. To date, mutations in no fewer than 17 genes coding for proteins expressed at EP are known to cause CMS (1): *ALG2* (MIM 607905), *ALG14* (MIM 612866), *CHRNA1* (MIM 100690), *CHRNB1* (MIM 100710), *CHRND* (MIM 100720), *CHRNE* (MIM 100725), *AGRN* (MIM 103320), *CHAT* (MIM 118491), *DPAGT1* (MIM 191350), *GFPT1* (MIM 138292), *LAMB2* (MIM 150325), *PLEC* (MIM 601282), *MUSK* (MIM 601296), *RAPSN* (MIM 601592), *COLQ* (MIM 603033), *SCN4A* (MIM 603967) and *DOK7* (MIM 610285). We here describe our findings in a novel CMS caused by mutations in the low-density lipoprotein receptor-related protein 4 encoded by *LRP4*.

EP development is triggered by the binding of agrin released from the nerve terminal to LRP4, a transmembrane protein of the

*To whom correspondence should be addressed at: Division of Neurogenetics, Center for Neurological Diseases and Cancer, Nagoya University Graduate School of Medicine, 65 Tsurumai, Showa-ku, Nagoya, Aichi 466-8550, Japan. Tel: +81 52 744 2446; Fax: +81 52 744 2449; Email: ohnok@med.nagoya-u.ac.jp (K.O.); Neuromuscular Research Laboratory, Department of Neurology, Mayo Clinic, 200 First Street SW, Rochester, MN 55905, USA. Tel: +1 507 284 5102; Fax: +1 507 2845831; Email: age@mayo.edu (A.G.E.)

postsynaptic membrane (2,3). LRP4 bound to agrin forms a ternary complex with the postsynaptic transmembrane muscle-specific receptor tyrosine kinase (MuSK). In this complex, the 3rd β-propeller domain of LRP4 is important for association with MuSK (4), although the interacting conformations remain unresolved. Binding of LRP4 to MuSK triggers phosphorylation and activation of the MuSK intracellular kinase domain. Activated MuSK in concert with Dok-7 stimulates rapsyn to concentrate and anchor AChR in the postsynaptic membrane and to interact with other proteins implicated in the assembly and maintenance of the NMJ (5). LRP4 was recently reported to provide a retrograde signal for presynaptic differentiation at neuromuscular junction (6,7). In addition, autoantibodies directed against LRP4 were recently recognized to cause a form of autoimmune myasthenia gravis (8–10).

In addition to its specific role at the NMJ, LRP4 is also a well-characterized inhibitor of the Wnt-signaling pathway. LRP4 signaling is involved in skeleton formation and kidney development. Mutations in *LRP4* have been reported in Cenani–Lenz syndactyly syndrome (CLSS) (11), sclerosteosis-2 (12), and low bone mineral density in human (13) and mice (14). Similarly, *Lrp4* mutations cause mule foot disease in cow (15) and kidney and limb defects in mouse (16). In addition, a missense SNP rs2306029 in *LRP4* is associated with 4.17-fold increase in the risk of developing Richter syndrome (17). To date, no report has implicated *LRP4* as a CMS disease gene.

Using Sanger and exome-capture resequencing, we identified two heteroallelic missense variants in *LRP4*, p.Glu1233Lys (c.3697G > A) and p.Arg1277His (c.3830G > A). Both variants are located at the edge of the 3rd β-propeller domain of LRP4. We show that each variant impairs binding ability of LRP4 for both agrin and MuSK as well as subsequent agrin-mediated phosphorylation and activation of MuSK, but neither mutation affects the Wnt-signaling pathway. Finally, by analysis of mutations in other diseases and by examining effects of artificially engineered mutations into the 3rd LRP4 β-propeller domain, we show the edge of this domain mediates the MuSK signaling, whereas its central cavity mediates the Wnt signaling.

RESULTS

Clinical data

The patient was born after 42 weeks of gestation with fetal distress and with Apgar scores of 3 and 6 at 1 and 5 min, respectively. Immediately after birth, she had a respiratory arrest and required hospitalization for feeding and respiratory support until the age of 6 months. She started to walk at 18 months but could only walk short distances. During childhood, she fatigued abnormally, could not climb step and was partially wheelchair dependent. Examination at the Mayo Clinic at ages 9 and 14 years revealed mild eyelid ptosis, slight limitation of lateral eye movements, moderately severe proximal greater than distal muscle weakness and hypoactive tendon reflexes. Repetitive nerve stimulation of the spinal accessory nerve showed a 13–16% decrement of the fourth compared with the first compound muscle action potential evoked from the trapezius, biceps and rectus femoris muscles with no significant decrement in the anterior tibial muscle. The decremental responses were transiently improved by edrophonium chloride, a fast acting cholinergic agonist. However, therapy for a few days with pyridostigmine at age 12 markedly worsened the patient's weakness. There was no history of similarly affected family members.

Endplate studies

An intercostal muscle specimen was obtained from the patient at age 17 years. Routine histologic examination revealed type 1 fiber preponderance. Synaptic contacts, examined in face-on views of glutaraldehyde-fixed AChE-reacted teased muscle fibers revealed multiple irregularly arrayed synaptic contacts that varied in shape and size (Fig. 1). None of the EPs had a normal pretzel shape. Electron microscopy examination of 54 EP regions of 29 EPs showed that the structural integrity of the nerve terminals and postsynaptic regions was preserved but quantitative analysis revealed that the size of the nerve terminals was reduced to 60%, and that of the postsynaptic region to 48%, of the corresponding control value (Table 1).

Immunofluorescence microscopy examination of frozen sections revealed normal expression of AChR and AChE at patient EPs. Ultrastructural localization of AChR at the EPs with peroxidase-labeled α-bungarotoxin (bgt) demonstrated normal distribution and density of AChR on the junctional folds. However, the total number of AChRs per EP fell slightly below the range of control values (Table 1).

The MEPP amplitude and the number of quanta released by nerve impulse fell in the normal range, and patch-clamp recordings from10 EPs revealed normal kinetics of the AChR channel (data not shown).

Sanger and exome-capture resequencing analysis

We analyzed the patient DNA using the exome-capture resequencing analysis. The number of SOLiD tags was 90.7×10^6

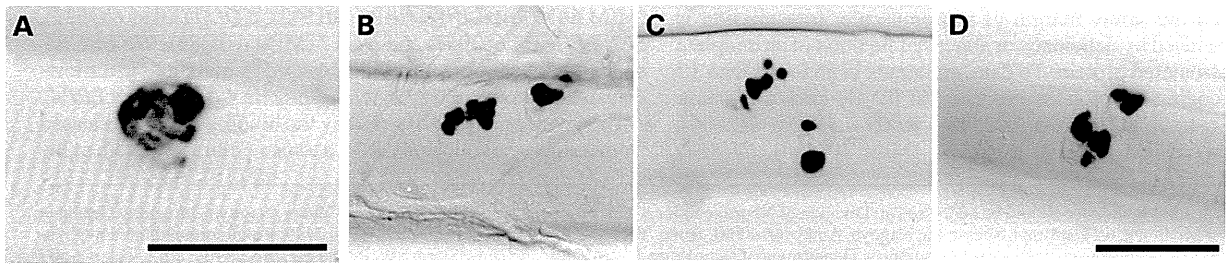

Figure 1. Synaptic contacts in intercostal muscle visualized by the cholinesterase reaction. (**A**) Normal EP. (**B–D**) Patient EPs. Note irregularly arrayed pleomorphic synaptic contacts at patient EPs. Bar in (A) indicates 50 μm. Bar in (D) indicates 50 μm for panels (B–D).

Table 1. Quantitative analysis of EP ultrastructure and [^{125}I]α-bungarotoxin-binding sites per EP

	Patient	Controls	*P*-value
Nerve terminal area (μm^2)	2.45 ± 0.30 (54)	3.88 ± 0.39 (63)	<0.005
Postsynaptic area (μm^2)	5.51 ± 0.45 (54)	10.6 ± 0.79 (59)	<0.001
[^{125}I]α-bgt-binding sites/EP	8.7×10^6	$12.82 \pm 0.79 \times 10^6$ (13) Range: 9.3–18.7	

Values represent mean ± SE. More than one region can occur at an EP. Values in parenthesis represent number of EP regions except for [^{125}I]α-bgt-binding sites where they indicate number of subjects. *P*-values are based on *t*-test.

spanning 4.53 Gb, and 72.8×10^6 tags (80.2%) spanning 3.47 Gb (76.6%) were mapped to the human genome hg19/GRCh37. As the SureSelect probes span 38 Mb, the mean coverage became 91.4. Among the 38-Mb SureSelect probe regions, 3.9% of nucleotides were not covered by any tags. Search for SNVs and indels using Avadis NGS with default parameters detected 46 555 SNVs/indels. We eliminated SNVs/indels registered in dbSNP137 and those with unreliable calls (Avadis decibel score ≤200), and obtained 4074 SNVs/indels. Restriction of our analysis to non-synonymous, frameshifting and splicing SNVs/indels in 33 candidate genes that are essential for the neuromuscular signal transmission yielded three SNVs. Among the three SNVs, a heterozygous c.1148C > G SNV predicting p.Ser376Arg in *SNTB2* encoding syntrophin β_2 was observed in a patient with periodic paralysis among our cohort of 31 patients other than CMS. In addition, 13 other missense SNPs and two frameshifting SNPs are registered in 539 codons encoded by *SNTB2* in dbSNP137. Thus, p.Ser376Arg in *SNTB2* was unlikely to be pathogenic. The two other SNVs were heterozygous c.3697G > A (chr11: 46 897 357) and c.3830G > A (chr11: 46 897 102) in *LRP4*, which predicted p.Glu1233Lys (EK mutation) and p.Arg1277His (RH mutation), respectively. Sanger sequencing of the patient's genomic DNA and mRNA confirmed both mutations and sequencing of cloned mRNA indicated that the mutations were heteroallelic. The father was heterozygous for p.Glu1233Lys. A half brother carried no mutation. No DNA was available from the mother. According to the PolyPhen-2 (18), SIFT (19) and Mutation Taster (20) algorithms, the predicted consequences of the EK mutation were 'benign', 'tolerated' and 'disease causing with $P > 0.99999$', respectively. Those of the RH mutation were 'probably damaging', 'affect protein function' and 'disease causing with $P > 0.99999$', respectively. LRP4 is a transmembrane protein with large extracellular domains (Fig. 2A). These mutations were in the 3rd low-density lipoprotein receptor (LDLR) type B repeat, known as β-propeller-like structure. The EK and RH mutations are downstream of the 4th and 5th YWTD motifs, respectively (Fig. 2B). The YWTD motifs are predicted to form the second β sheet below the surface β sheet of each blade of the 3rd β-propeller domain, and the mutations are at the linker between the surface β sheet and the second β sheet.

The EK and RH mutations in *LRP4* impair the MuSK signaling pathway

During the NMJ formation, binding of agrin to LRP4 induces phosphorylation and activation of MuSK, which activates ATF2 downstream of JNK and induces clustering of AChR. To study effects of the mutations in this signaling pathway, we used a JNK-responsive ATF2-luciferase (ATF2-luc) reporter (21), which specifically monitors MuSK-dependent stimulation in transfected HEK293 cells. Overexpression of LRP4 and MuSK activated the ATF2-luc reporter in the absence of agrin, as previously reported (22). The EK mutant minimally and the RH mutant moderately impaired LRP4-induced activation of ATF2-luc (Fig. 3A). Addition of agrin to the medium markedly enhanced the ATF2-luc activity for the wild-type LRP4, whereas both mutants completely abolished responsiveness to agrin (Fig. 3A).

We also examined effects of the mutations on MuSK phosphorylation that occurs immediately after formation of the agrin/LRP4/MuSK complex. Consistent with its effects on the signaling activity, agrin enhanced MuSK phosphorylation in the presence of wild-type LRP4 but not in the presence of mutant LRP4 in HEK293 cells (Fig. 3B) and in Lrp4-downregulated C2C12 myoblasts (Fig. 4B). Similarly, wild-type LRP4, but not EK and RH mutants, rescued AChR clustering in Lrp4-downregulated C2C12 myotubes (Fig. 4C). These results support the notion that the EK and RH mutations compromise agrin-mediated activation of MuSK and AChR clustering.

LRP4 has also been known as an extracellular antagonist for Wnt signaling. Wnt signaling is involved in tissue development including limb, bone and kidney. Indeed, previously reported mutations of *LRP4* in human, mouse and cow exhibit structural abnormalities in limb, bone and/or kidney. We thus examined the effects of our LRP4 mutations on Wnt-signaling pathway using the TOPFLASH reporter. Wild-type LRP4 suppressed the Wnt3a-mediated TOPFLASH activity, and the EK and RH mutations retained similar suppressive effects (Fig. 3C). Lack of limb, bone and kidney symptoms in our patient can be attributed to EK and RH only affecting agrin-induced activation of MuSK but having no effect on Wnt signaling.

LRP4 directly binds to agrin and MuSK through its extracellular domain. To test the effects of the LRP4 mutations on binding to MuSK and agrin, we performed cell surface-binding assays. We first confirmed that the EK and RH mutants had no effect on LRP4 expressions in cell body and cell membrane in COS7 cells (Supplementary Material, Fig. S1). MuSKect-mycAP (Fig. 5A) and agrin-mycAP (Fig. 5B) bound efficiently to wild-type LRP4 expressed on the surface of COS7 cells. The RH and EK mutants compromised binding of both MuSKect-mycAP and agrin-mycAP (Fig. 5A and B). We also analyzed direct binding of LRP4ecd-Flag to purified MuSKect-mycAP (Fig. 5C) and agrin-mycAP (Fig. 5D) by *in vitro* plate-binding assays (Fig. 5E and F). We found that the mutations decreased binding affinities of LRP4 for agrin-mycAP (Fig. 5E) and MuSKect-mycAP (Fig. 5F). The RH mutant compromised binding of agrin and MuSK more than the EK mutant in the cell surface-binding assay but not in the *in vitro* plate-binding assay, which may be accounted for by some other molecules

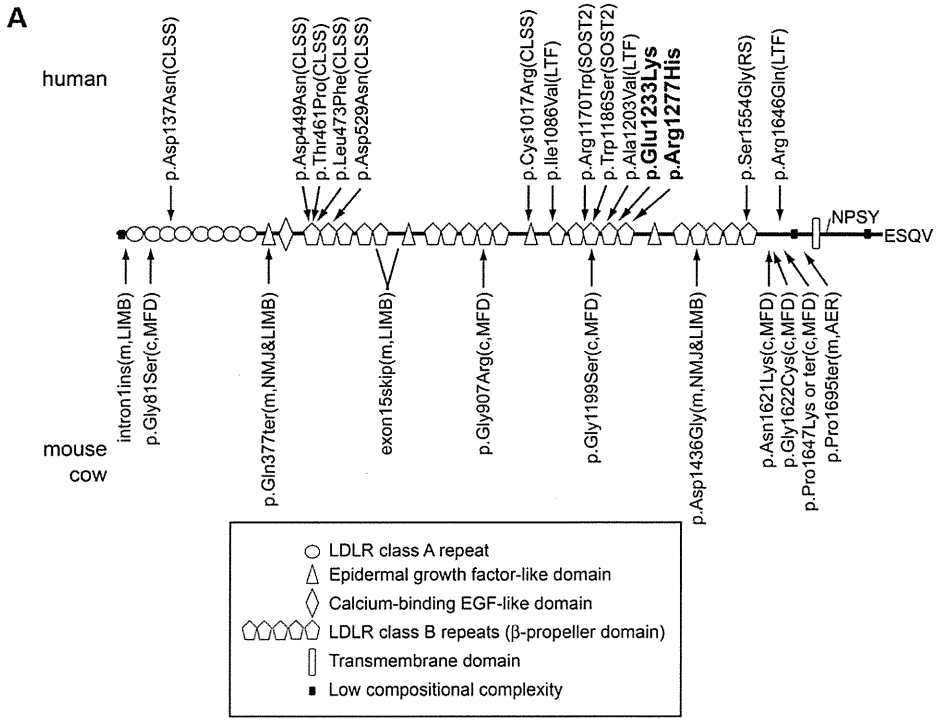

B

4th YWTD motif in 3rd LDLR type B repeat

p.Glu1233Lys

```
Homo sapiens.tx 1205 LINNNLGWPNGLTVDKASSQLLWADAHTERIEAADLNGANRHTLVSPVQHPYGLTLLDSY 1264
Bos taurus.txt  1205 LINSNLGWPNGLTVDKASSQLLWADAHTERIEAADLNGANRHTLVSPVQHPYGLTLLDAY 1264
Canis familiari 1321 LISNNLGWPNGLTVDKASSQLLWADAHTERIEAADLNGGSRHTLVSPVQHPYGLTLLDSY 1380
Rattus norvegic 1205 LINNNLGWPNGLTVDKTSSQLLWADAHTERIEVADLNGANRHTLVSPVQHPYGLTLLDSY 1264
Mus musculus.tx 1205 LINNNLGWPNGLTVDKTSSQLLWADAHTERIEVADLNGANRHTLVSPVQHPYGLTLLDSY 1264
Gallus gallus.t 1249 LISNNLGWPNGLAVDKAGSQLLWADAHTERIEAADLNGANRRTLLSPVQHPYGLTLLDSY 1308
Tetraodon nigro 1025 LISNNLGWPNGLAIDTAGSQLLWADAHTERIEAADLNGQNRRTLVTPVQHPYGLTLLGSH 1084
Drosophila mela 1381 IVTANLGWPNGLSLDLKSKRIYWVDARLKTIDSCDYTGNQRKLIMSSLHHPYALALSDDN 1440
Aedes aegypti.t 1422 IVTTDLGFVSGLAVDSVENRIYWTDSKAKRIESCDFNGNSRKILLNNLSHPYALTVTTST 1481
                      ..   **   **..*    .. * *..   *. .* .*  *. ..  . *** *..
```

5th YWTD motif in 3rd LDLR type B repeat

p.Arg1277His

```
Homo sapiens.tx 1265 IYWTDWQTRSIHRADKGTGSNVILVRSNLPGLMDMQAVDRAQP--LGFNKCGSRNGGCSH 1322
Bos taurus.txt  1265 IYWTDWQTRSIHRADKGTGSNVILVRSNLPGLMDIQAVDRSQP--LGVNKCGPRNGGCSH 1322
Canis familiari 1381 IYWTDWQTRSIHRADKGTGSNVILVRSNLPGLMDIQAVDRAQP--LGFNKCGSRNGGCSH 1438
Rattus norvegic 1265 IYWTDWQTRSIHRADKSTGSNVILVRSNLPGLMDIQAVDRAQP--LGFNKCGSRNGGCSH 1322
Mus musculus.tx 1265 IYWTDWQTRSIHRADKSTGSNVILVRSNLPGLMDIQAVDRAQP--LGFNKCGSRNGGCSH 1322
Gallus gallus.t 1309 IYWTDWQTRSIHRADKDSGANVILVRANLPGLMDIQAVDRARP--LGFNKCGVRNGGCSH 1366
Tetraodon nigro 1085 IYWTDWQSRSIQRADKTTGTNTITVRSNLPGLMDIQAVDMERP--LGFNKCGRRNGGCTH 1142
Drosophila mela 1441 IYWTDWKSKALHMTERRNISAKRDIITNIDGLMDIKIIYQNQNQSTMKNACGNNNGNCSH 1500
Aedes aegypti.t 1482 VYWTDWVTKALHSVSKLNTSKVRKVAKDLEELMDVKVVLGPSD--SQDDFCGKNNGGCSH 1539
                     .*****  .....   .   .   .   .  ***.. .           **  **.*.*
```

Figure 2. Structure and previously identified mutations of LRP4. (**A**) Domain structure of LRP4 and positions of reported mutations in human, mouse and cow. p.Glu1233Lys (EK mutation) and p.Arg1277His (RH mutation) in the current studies are shown in bold. In human, LRP4 mutations cause CLSS (MIM 212780) and sclerosteosis-2 (SOST2, MIM 614305). SNPs are also associated with an increased risk for Richter syndromes (RS) and a low-trauma fracture (LTF) due to decreased bone mineral density. In mouse, mutations cause abnormal development of the apical ectodermal ridge (AER) leading to polysyndactyly and tooth abnormality, as well as abnormal developments of limbs (LIMB) and the neuromuscular junctions (NMJ). In cow, mutations lead to mulefoot disease (MFD). LRP4 harbors eight low-density lipoprotein receptor (LDLR) domain class A, four epidermal growth factor-like domains, a calcium-binding EGF-like domain, four LDLR class B repeat (β-propeller domain), a transmembrane domain and an intracellular domain. The LDLR type B repeat contains five tandem repeats of an YWTD motif to build a propeller-like structure. NPSY close to the C-terminal end is a motif for endocytosis and ESQV at the C-terminal end is a motif for binding to PDZ-containing proteins. (**B**) Positions of the EK and RH mutations downstream of the 4th and 5th YWTD motifs (boxed). The amino acid sequences are highly conserved across vertebrates but not in insects. Asterisks indicate strictly conserved amino acids, and dots indicate loosely conserved amino acids.

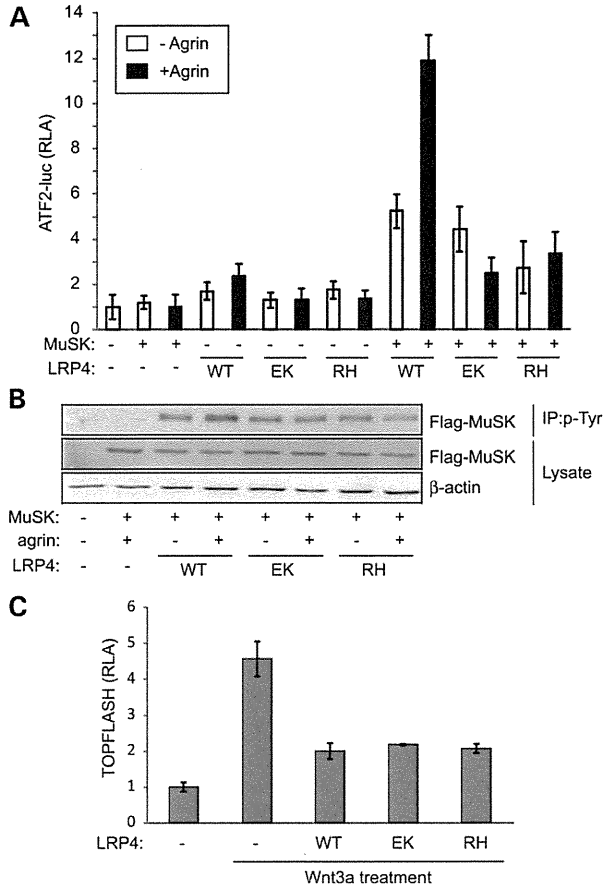

Figure 3. p.Glu1233Lys (EK) and p.Arg1277His (RH) mutants compromise agrin-mediated upregulation of MuSK signaling but retain Wnt-suppressive activity in HEK293 cells. (**A**) ATF2-luciferase reporter assay of HEK293 cells to quantify agrin-mediated activation of the MuSK signaling pathway. Cells were transfected with ATF2-luc reporter and Renilla reporter plasmids along with MuSK cDNA and the indicated LRP4 cDNA. Cells were cultured with or without 10 ng/μl agrin. Wild-type (WT) LRP4-activated MuSK without agrin, and agrin further enhanced the activation. The EK and RH mutations compromise MuSK activation in the presence or absence of agrin. (**B**) MuSK phosphorylation assay of HEK293 cells transfected with Flag-MuSK and the indicated *LRP4* cDNA with or without agrin (10 ng/μl). Phosphorylated MuSK was detected by immunoprecipitation of cell lysate by anti-phosphotyrosine antibody (p-Tyr) followed by immunoblotting with anti-FLAG antibody. Wild-type LRP4 phosphorylates MuSK, which is further enhanced by agrin, but EK and RH mutants abolish responsiveness to agrin. (**C**) TOPFLASH reporter assay of HEK293 cells to quantify responsiveness to Wnt3a. Cells were transfected with the TOPFLASH reporter and Renilla reporter plasmids along with the indicated *LRP4* cDNA. Cells were cultured in the presence or absence of Wnt3a. Means and SD are indicated. Wild-type (WT) and mutant LRP4 (EK and RH) suppress the Wnt3a-mediated signaling to the same extent.

expressed on the cell surface, beneath the cell membrane or secreted from the cells.

Mutations in *LRP4* causing sclerosteosis-2 have No effect on MuSK signaling

In contrast to our EK and RH mutations in the 3rd β-propeller domain, p.Arg1170Trp (abbreviated as RW) and p.Trp1186Ser (WS) mutations identified in a patient with sclerosteosis-2 impair Wnt-suppressing activity of LRP4 (12). We first confirmed that wild-type LRP4 and the two mutants are similarly expressed on the plasma membrane in HEK293 cells (Fig. 6A) as we observed in COS7 cells (Supplementary Material, Fig. S1). We then analyzed the effects of the two mutations on MuSK (Fig. 6B) and Wnt (Fig. 5C) signaling. Consistent with the previous report (12), the RW and WS mutations abrogated the Wnt-suppressing activity of LRP4 (Fig. 6C) but had no effect on agrin-induced MuSK signaling (Fig. 6B). Cell surface-binding assay also confirmed that the two mutants retained their ability to bind to agrin and MuSK (Fig. 6D).

As the four mutations affecting MuSK or Wnt signaling were all in the 3rd β-propeller domain, we scrutinized the positions of mutations by homology modeling of the 3rd β-propeller domain of human LRP4 using the 1st β-propeller domain of human LRP6 (PDB ID: 3SOV). The 3rd β-propeller domain contains six blade-like structures and displays a YWTD motif at the second β sheet below the surface of each blade (Fig. 7A and Supplementary Material, Movie S1). In this model, the EK and RH mutations, which only affect agrin/LRP4/MuSK signaling, are located on edge of the 5th and 6th blades, respectively (Fig. 7B and Supplementary Material, Movie S1). In contrast, the RW and WS mutations, which only affect Wnt signaling, are located in a central cavity of the propeller (Fig. 7C and Supplementary Material, Movie S1).

Artificially engineered Lrp4 mutations at the edge of the 3rd β-propeller domain affect MuSK signaling and those in the central cavity affect Wnt signaling

To further confirm that the edge of the 3rd β-propeller domain mediates MuSK signaling and that the central cavity mediates Wnt signaling, we introduced four other artificial mutations based on structural modeling of the 3rd β-propeller domain (Fig. 7A and Supplementary Material, Movie S1). As RH and EK mutations affected two exposed amino acids on the 2nd β sheet, we introduced an alanine into two neighboring amino acids to make IA and VA mutations (Fig. 7B and Supplementary Material, Movie S1). Similarly, as WS and RW mutations were facing the central cavity of the 3rd β-propeller domain, we introduced an alanine into the corresponding amino acids in the other blades to make YA and NA mutations (Fig. 7C and Supplementary Material, Movie S1). We then examined the effects of each mutation on MuSK and Wnt signaling. As expected, the VA and IA mutations at the edge of the 3rd β-propeller domain affected MuSK signaling (Fig. 8A), but not Wnt signaling (Fig. 8B). In contrast, the NA and YA mutations in the central cavity normally activated MuSK signaling (Fig. 8A), but lost Wnt-suppressive activity (Fig. 8B). Similarly, the cell surface-binding assay showed that the VA and IA mutations reduced binding of agrin and MuSK (Fig. 8C and D). Thus, the artificial mutations further underscore the differential signaling roles of the edge and the central cavity of the 3rd β-propeller domain.

DISCUSSION

LRP4 mutations cause a novel CMS

Because mutations in *AGRN* (25) and *MUSK* (26) have been known to cause CMS and because LRP4 was shown to be a

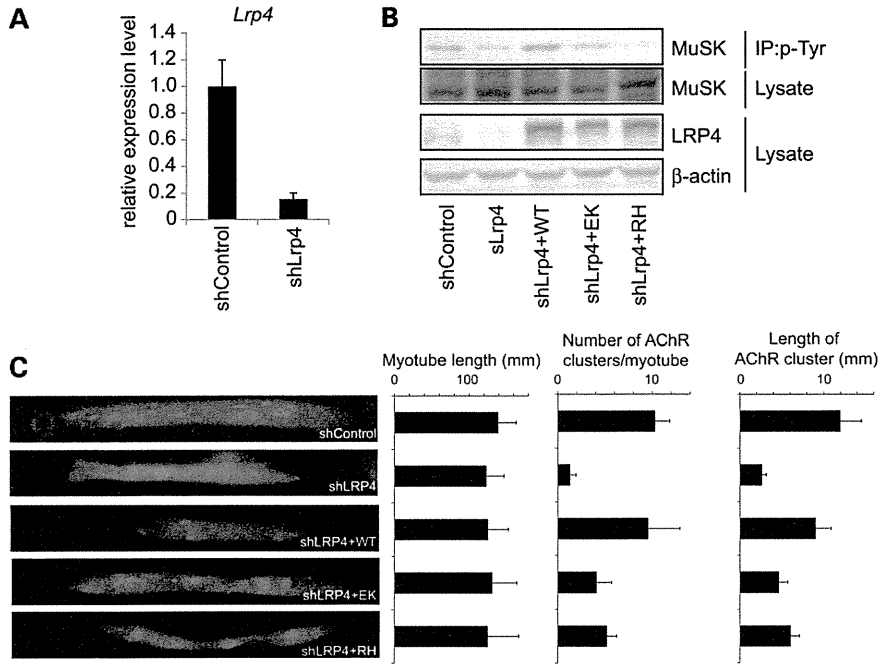

Figure 4. p.Glu1233Lys (EK) and p.Arg1277His (RH) mutants compromise agrin-mediated upregulation of MuSK signaling and AChR clustering in C2C12 myoblasts/myotubes. (**A**) Endogenous Lrp4 expression in C2C12 myoblasts is suppressed by shRNA against mouse Lrp4 (shLrp4) by qRT-PCR. (**B**) MuSK phosphorylation assay of differentiation-induced C2C12 myoblasts transfected with shControl or shLrp4 and the indicated *LRP4* cDNA. Phosphorylated MuSK was detected by immunoprecipitation of cell lysate by anti-phosphotyrosine antibody (p-Tyr) followed by immunoblotting with anti-MuSK antibody. Wild-type LRP4, but not EK and RH mutants, phosphorylates MuSK in Lrp4-deficient myoblasts. (**C**) Agrin-mediated AChR clustering in C2C12 myotubes. Myotubes are transfected with EGFP cDNA, shLRP4 and the indicated *LRP4* cDNA using electroporation. AChR is visualized with Alexa594-conjugated α-bungarotoxin at 12 h after adding 10 ng/ml agrin. Right panels: Morphometric analysis showing that wild-type (WT) LRP4, but not EK and RH mutants, rescues the number and the length of AChR clusters in Lrp4-downregulated C2C12 myotubes. LRP4 has no effect on myotube length.

coreceptor for agrin that mediates activation of MuSK (Fig. 7D) (2,3). *LRP4* has been a candidate gene for a CMS for a number of years. In this communication, we show that mutations in *LRP4* cause a CMS and that the identified mutations affect MuSK signaling by compromising binding of LRP4 to both agrin and MuSK.

Our data predict that the identified *LRP4* mutations interfere with agrin-LRP4-MusK signaling and thereby hinder concentration of AChR on the junctional folds as well as normal development and maintenance of the entire junction. Our EP studies show that the synaptic contacts are dysplastic (Fig. 1) and that the nerve terminal and postsynaptic areas at the EP regions are hypoplastic (Table 1), but the AChR content of EPs and the synaptic response to ACh are not appreciably reduced. Because the patient has a myasthenic disorders by clinical and EMG criteria, we attribute sparing of the intercostal muscles to different expressivity of the genetic defect in different muscles. Sparing of selected muscles can occur in both autoimmune and congenital myasthenias and is indicated by absence of muscle weakness or a decremental EMG response from some muscles in either disorder. For example, in MuSK antibody-positive myasthenia, EPs in intercostal and biceps brachii muscles have a normal AChR content, generate normal MEPP amplitudes, and have well preserved junctional folds (27,28). Analysis of *Musk* and *Lrp4* expressions in mouse muscles by quantitative RT–PCR revealed that expressions of *Musk* in omohyoid and trapezius muscles were less than those in the other muscles (Supplementary Material, Fig. S2). The least expression of *Musk* in mouse omohyoid has been recently reported (29). In contrast, *Musk* expression in intercostal muscle was ~three times more compared with omohyoid. Although human specimens of various muscles were not available for our studies, high and low MuSK expressions in intercostal and trapezius muscles may partly account for spared and impaired NMJ signal transmissions in intercostal and trapezius muscles, respectively, in our patient with *LRP4* mutations.

Position-specific disease phenotypes of *LRP4* mutations

The extracellular domain of LRP4 is known to bind to several proteins: agrin (2,3), MuSK (4), Wnt ligands (30), dkk1 (31), a Wnt inhibitor (32,33), sclerostin (31), another Wnt inhibitor (32,33) and possibly apoE (34). Specific binding domains of LRP4 have been dissected: agrin binds to the LDLa repeats 6–8, EGF-like domains, and the 1st β-propeller domain (Fig. 7B and Supplementary Material, Movie S1) (4,23); MuSK binds to the 4th/5th LDLa repeats and the 3rd β-propeller domain (4); sclerostin binds to the 3rd β-propeller domain (12); and apoE binds to LDLa (34). As for Wnt ligands, the precise molecular mechanisms how LRP4 suppresses Wnt signaling remain elusive, although the Wnt-suppressive effect of LRP4 is well established (35).

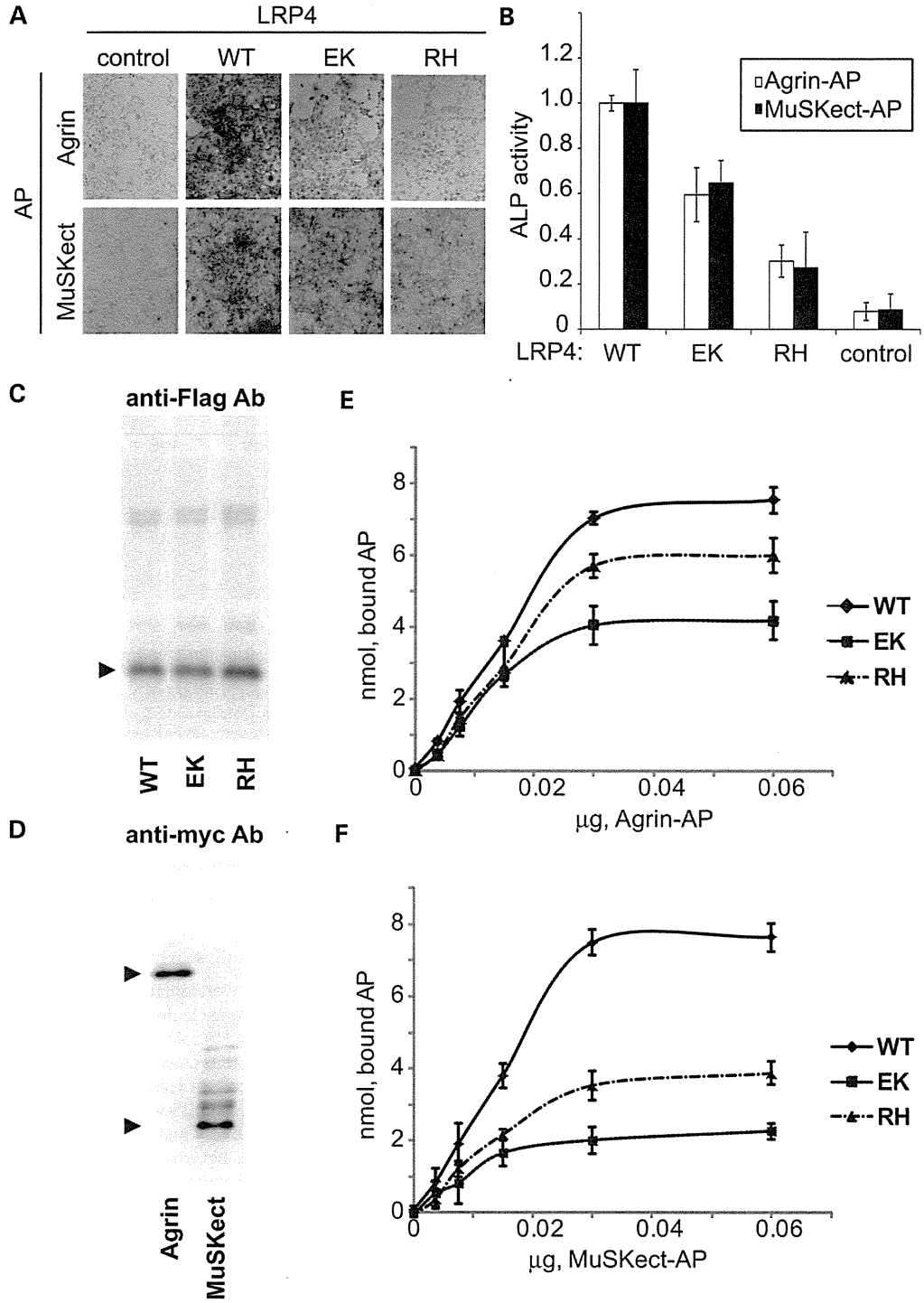

Figure 5. The p.Glu1233Lys (EK) and p.Arg1277His (RH) mutants impair binding of LRP4 to MuSK and agrin. (**A** and **B**) Cell surface-binding assays. COS7 cells were transfected with the wild-type or mutant *LRP4* cDNA and added with concentrated conditioned medium containing either neural Agrin-mycAP or MuSKect-mycAP as indicated. Control cells were transfected with an empty vector. Bound MuSKect-mycAP or agrin-mycAP was stained for the alkaline phosphatase activity (A). (B) The mean and SD of ALP activities of bound agrin-mycAP and MuSKect-mycAP in three independent wells. The RH and EK mutants reduce binding of MuSKect-mycAP and agrin-mycAP. (**C** and **D**) Western blotting with an anti-Flag antibody for detecting LRP4ecd-Flag; and anti-myc antibody for agrin-myc and MuSK-myc. All the transfected cDNAs were similarly expressed. (**E** and **F**) *In vitro* plate-binding assays. Plates were coated with the wild-type or mutant LRP4ecd-Flag protein and overlaid with purified agrin-mycAP protein (E) and MuSKect-mycAP (F). The EK and RH mutants reduce binding affinities for MuSKect-mycAP and agrin-mycAP. Mean and SE are plotted ($n = 4$; $P < 0.05$ for both MuSKect-mycAP and agrin-mycAP by two-way ANOVA).

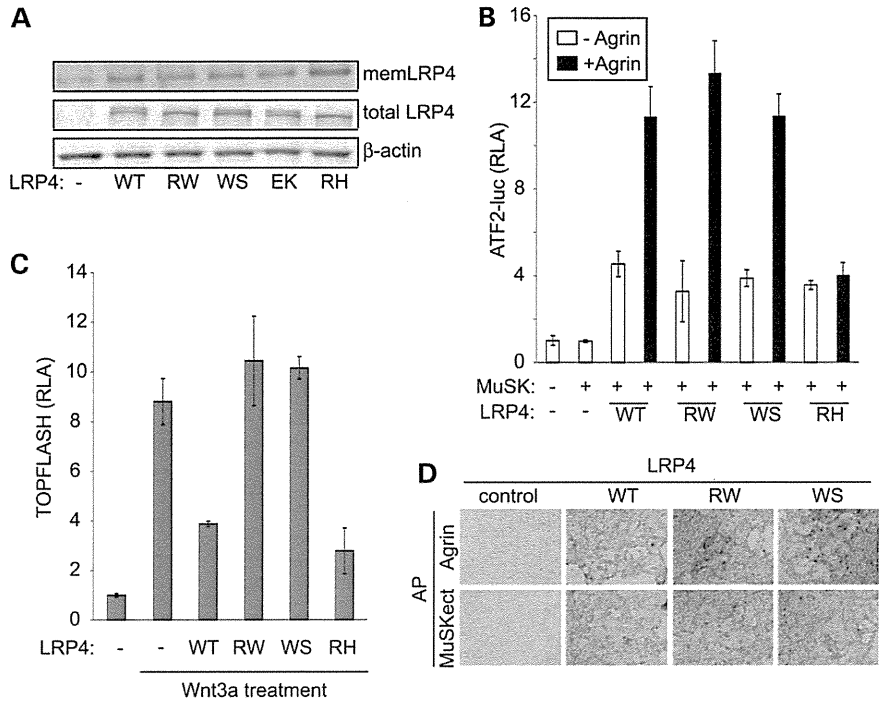

Figure 6. The p.Arg1170Trp (RW) and p.Trp1186Ser (WS) mutants retain the activity of agrin-mediated upregulation of MuSK signaling but compromise Wnt-suppressive activity. (**A**) Western blotting with an anti-Flag antibody for detecting full-length LRP4-Flag. Membrane proteins are biotinylated and precipitated with streptavidin. β-Actin proteins in each sample were detected as loading control. (**B** and **C**) ATF2-luciferase (B) and TPOFLASH (C) reporter assays of HEK293 cells to quantify activation of MuSK and Wnt signaling pathways, respectively. The RH mutant is included as a control. Means and SD of three independent experiments are indicated. (**D**) Cell surface-binding assays as in Figs 5A and B. Both the RW and WS mutants are able to bind to agrin-mycAP (upper) and MuSKect-mycAP (lower).

The diverse array of binding partners enables LRP4 to play an essential role in multiple biological processes including limb and kidney morphogenesis (16,31); bone development through cell fate decision and migration (35); and synaptogenesis (6,34). The multiple phenotypes caused by mutations in the 3rd β-propeller domain prompted us to scrutinize different regions of this domain, and we found that the edge mediates MuSK signaling and the central cavity mediates Wnt signaling. That a single missense mutation in the 3rd β-propeller domain compromises LRP4 binding to MuSK supports a previous observation that MuSK is bound to the 3rd β-propeller domain of LRP4 (Fig. 7B and Supplementary Material, Movie S1) (4). In contrast, reduced binding of our LRP4 mutants to agrin was unexpected because agrin binds to the EGF-like domain, LDLa repeats 6–8 and the 1st β-propeller domain (4,23). The 2nd and 3rd β-propeller domains, however, enhance binding to agrin to ~170% of the truncated LRP4 lacking these domains (4). Accordingly, mutations in the 3rd β-propeller domain in our patient are likely to compromise the enhancing effect conferred by the 3rd β-propeller domain of LRP4.

MATERIALS AND METHODS

Patient

All human studies were in accord with and approved by the Institutional Review Boards of the Mayo Clinic and Nagoya University Graduate School of Medicine. The patient's father gave informed consent for the patient to participate in the study. Venous blood sample was obtained from the patient and his father and genomic DNA was isolated with the QIAamp Blood DNA kit (Qiagen) according to the manufacturer's recommendations.

Neuromuscular junction studies

Intercostal muscle specimens were obtained from the patient and from control subjects without muscle disease undergoing thoracic surgery. Cryosections were used to colocalize the acetylcholine receptor (AChR) and acetylcholine esterase (AChE) as described (36). AChE was also visualized on teased, glutaraldehyde-fixed muscle fibers cytochemically (37). EPs were localized for electron microscopy (38) and quantitatively analyzed (39) by established methods. Peroxidase-labeled α-bgt was used for the ultrastructural localization of AChR (40). The number of AChRs per EP was measured with [^{125}I]α-bgt. The amplitude of the miniature EP potential (MEPP) and EP potential (EPP) amplitudes and estimates of the quantal content of the EPP (*m*) were measured as previously described (41,42). Single-channel patch-clamp recordings were performed as previously described (43,44).

Exome-capture resequencing analysis

We enriched exonic fragments using the SureSelect human all exon v2 (Agilent Technologies) and sequenced 50 bp of each

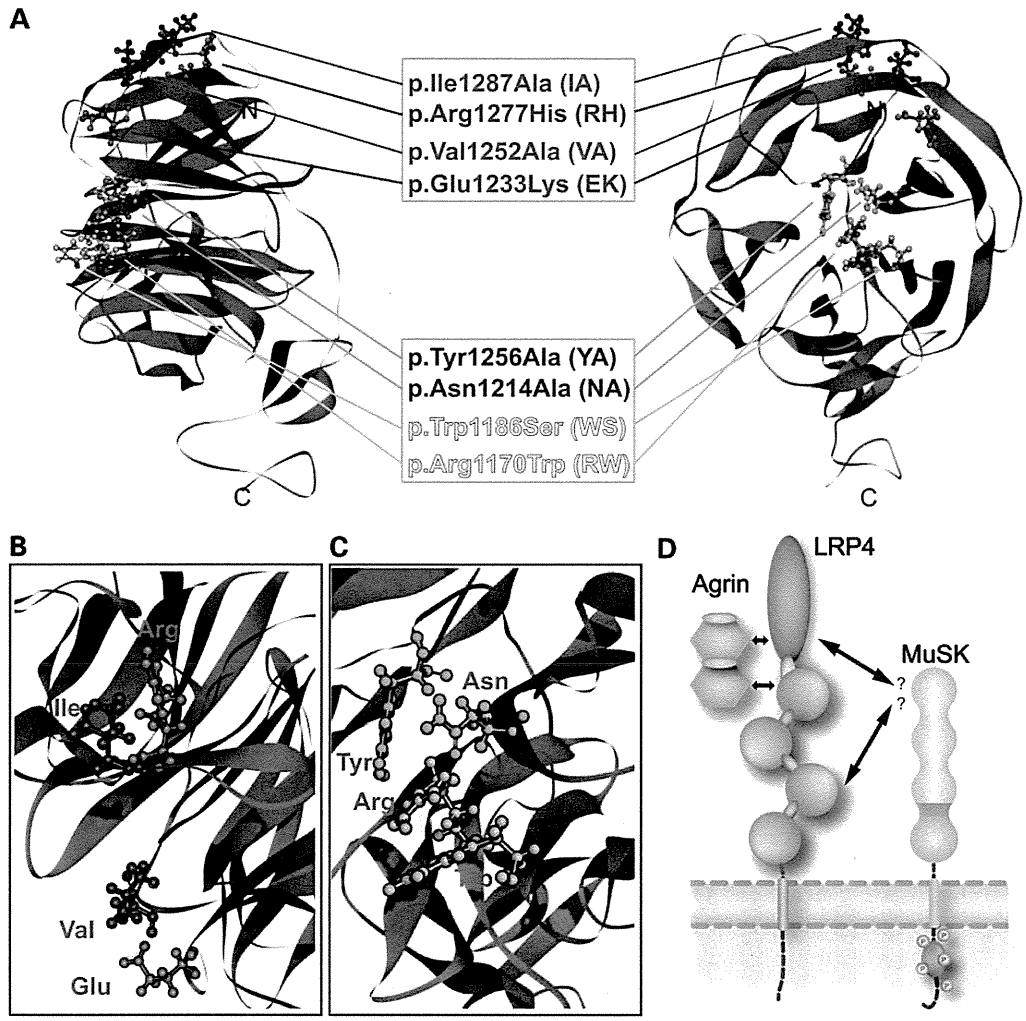

Figure 7. The 3rd β-propeller domain of LRP4 and scheme of agrin/LRP4/MuSK complex. (**A**–**C**) Simulated three-dimensional structure of the 3rd β-propeller domain of LRP4. Positions of the analyzed mutations are indicated. The RH and EK mutations (red) are identified in our CMS patient. The RW and WS mutations (yellow) are reported in sclerosteosis-2 (12). Amino acids that are artificially mutated to alanine are shown in purple or green. Mutations at the edge of the β-propeller domain and in the central cavity are grouped together by boxes. The edge (B) and central cavity (C) of the 3rd β-propeller domain are enlarged to show locations of the naturally occurring and artificially introduced mutations. The viewing positions of (B) and (C) are not identical to (A). (**D**) Scheme of agrin/LRP4/MuSK. Arrows represent direct interactions: Agrin binds to the 1st EGF-like domain and the 1st β-propeller domain of LRP4 (23); MuSK binds to the 4th/5th LDLa repeats and the 3rd β-propeller domain of LRP4 (4). An artificial missense mutation in the 1st IgG-like domain of MuSK impairs binding to LRP4 (4) and deletion of this domain abolishes agrin-mediated AChR clustering (24), but the exact LRP4-binding domain(s) of MuSK remain elusive. We propose that the edge of the 3rd β-propeller domain of LRP4 is essential for binding to MuSK and for signal transduction at NMJ.

fragment in a single direction using ABI SOLiD4 system (Life Technologies). The sequencing fragments were mapped to the human genome hg19/GRCh37 using BioScope 1.4 (Life Technologies). SNVs/indels were called by Avadis NGS 1.3.1 (Agilent) using default parameters. We restricted our analysis to 34 candidate genes that were known to be essential for neuromuscular signal transmission: *ABL2*, *ACHE*, *AGRN*, *APP*, *CHAT*, *CHRNA1*, *CHRNB1*, *CHRND*, *CHRNE*, *CHRNG*, *COLQ*, *CSNK2B*, *DAG1*, *DOK7*, *DTNA*, *DVL1*, *ETV5*, *GFPT1*, *LAMB2*, *LRP4*, *MUSK*, *NRG1*, *NTF4*, *PAK1*, *PGGT1B*, *PHLDB2*, *PLEC*, *RAPSN*, *SCN4A*, *SLC18A3*, *SNTB2*, *STNA1* and *SYNC*.

Primer pairs for each exon and the flanking intron regions of *LRP4* were designed with Primer 3. PCR products were directly sequenced with ABI PRISM 3730 DNA Analyzer and BigDye Terminator Cycle Sequencing Kit version 1.1 according to the manufacturer's protocols (Applied Biosystems).

Plasmids

Full-length human *LRP4* cDNA (Open Biosystems) was cloned into the *Eco*RI site of the pcDNA3.1 mammalian expression vector. The extracellular domain (amino acid 1–1722) of

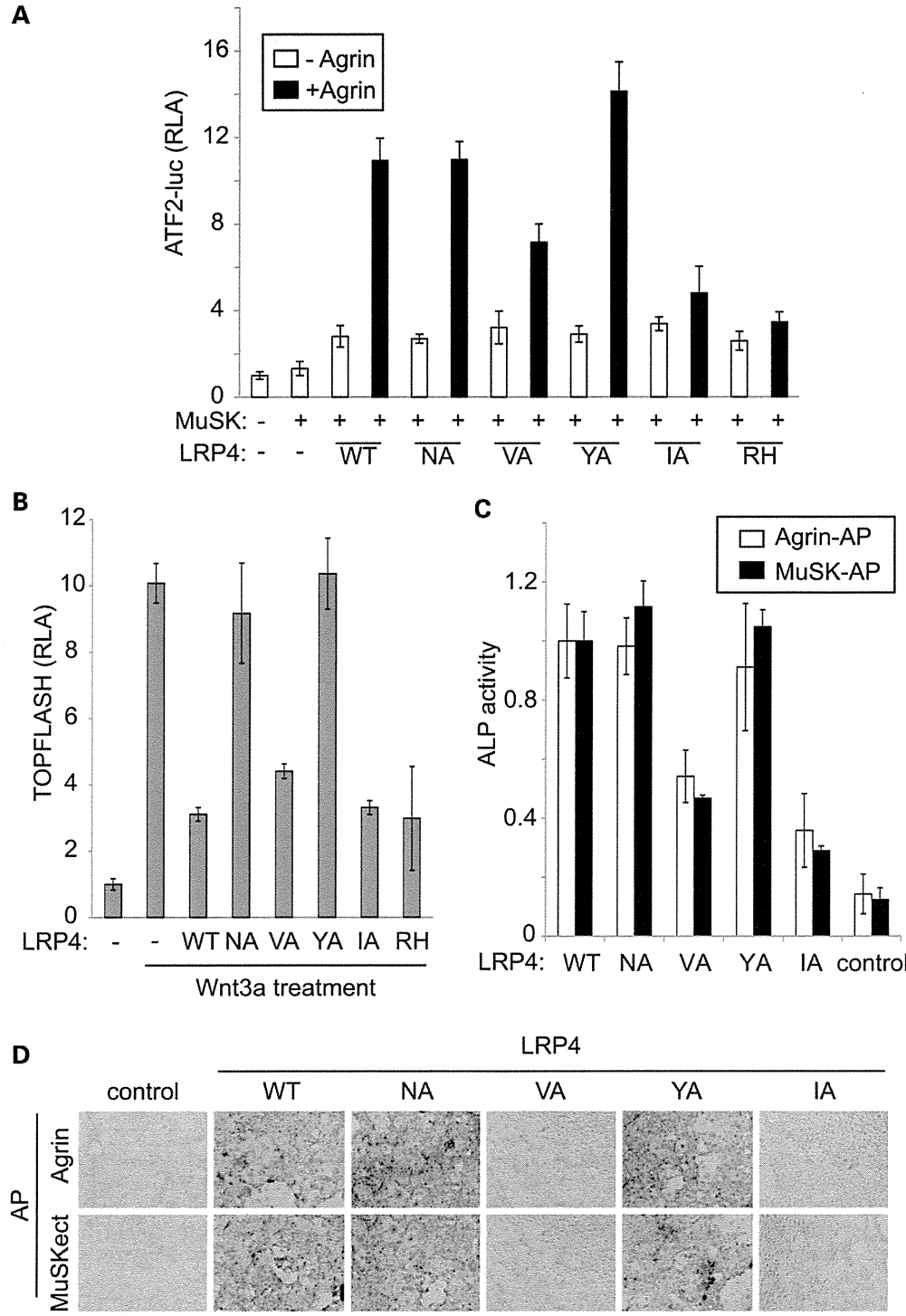

Figure 8. Artificially engineered p.Val1252Ala (VA) and p.Ile1287Ala (IA) compromise agrin-mediated upregulation of MuSK signaling, whereas p.Asn1214Ala (NA) and p.Tyr1256Ala (YA) compromise Wnt-suppressive activity. (**A**) ATF2-luciferase reporter assay of HEK293 cells as in Figs 3A and 6B. The IA and VA mutations are at the edge, whereas the YA and NA mutations are in the central cavity (see Fig. 7A and Supplementary Material, Movie S1). The RH mutation in our CMS patient is included as a control. (**B**) TOPFLASH reporter assay of HEK293 cells as in Figs 3C and 6C. (**C and D**) Cell surface-binding assays as in Figs 5A, B, and 6D. The ALP activities of bound agrin-mycAP and MuSKect-mycAP in three independent wells are shown in (C). Mean and SD are indicated in (A)–(C).

human *LRP4* cDNA was cloned into the *Hin*dIII and *Xba*I sites upstream of a 3xFlag epitope of a mammalian expression vector p3xFlag-CMV-14 to generate hLRP4ecd-Flag for the plate-binding assay. The mouse *Musk* cDNA in pExpress-1 was purchased from Open Biosystems and was used for the luciferase assay in HEK293 cells. Human *MUSK* cDNA with a Flag-tag at the N-terminal end was cloned into the *Eco*RI and *Xba*I sites of the p3xFlag-CMV-14 to generate Flag-MuSK, and was used for the co-immunoprecipitation assay. For vector expressing shRNA against Lrp4, double-stranded oligonucleotides (sense, 5′-GATCCCGGAAGTTTCCTGACATAAATTCAAGAGAT TTATGTCAGGAAACTTCCTTTTGGAAA-3′ and 5′-AGCT TTTCCAAAAAGGAAGTTTCCTGACATAAATCTCTTGAA TTTATGTCAGGAAACTTCCGG-3′) were cloned into a lentiviral vector pLenti-CMV-GFPx2-DEST, which was kindly provided by Dr Eric Campeau at the University of Massachusetts Medical School. The extracellular domain of mouse *Musk* cDNA fused to a myc-tag and alkaline phosphatase (MuSKect-mycAP) was kindly provided by Dr Lin Mei. To generate rat agrin-mycAP that retains potency to facilitate AChR clustering as a neural agrin, we cloned amino acid 1141–1937 of rat *Agrn* cDNA (M64780.1) into pAPtag-5 (GenHunter) at the *Hin*dIII and *Sna*BI sites, so that the Igk-originated signal peptide is attached upstream of the insert and the myc-tag/alkaline phosphatase downstream. Mutant *LRP4* plasmids carrying p.Arg1170Trp, p.Trp1186Ser, p.Asn1214Ala, p.Glu1233Lys, p.Val1252Ala, p.Tyr1256Ala, p.Arg1277His and p.Ile1287Ala were generated by the QuikChange Site-Directed Mutagenesis kit (Stratagene). Lack of PCR artifacts was verified by sequencing the entire inserts. Super 8x TOPFLASH plasmid (Addgene), ATF2-Luc (21) and phRL-TK Renilla luciferase vector (Promega) were used for the luciferase reporter assay.

Cell cultures

HEK293, L, COS and C2C12 cells were cultured in the Dulbecco's modified Eagle's medium (DMEM) supplemented with 10% fetal calf serum and transfected with FuGENE 6 transfection reagent (Roche). L cells stably expressing Wnt3a were purchased from ATCC. Conditioned media were prepared by culturing Wnt3a-producing and control L cells for 4 days. The LRP4ecd-Flag, agrin-mycAP and MuSKect-mycAP proteins were produced by transfecting each plasmid into HEK293 cells in serum-free DMEM. Recombinant rat C-terminal agrin (10 ng/ml, R&D systems) was used for agrin treatment except for the binding assays. For AChR clustering assay, C2C12 myoblast were seeded on a plate coated with collagen I (BD Biosciences) and differentiated in DMEM supplemented with 2% horse serum for 5 days. The differentiated myotubes were electroporated with shLrp4 and each LRP4 cDNA construct using the NEPA21 electroporator and the CUY900-13-3-5 electrode for attached cells (NepaGene), and then treated with 2 μg/ml doxycycline for 2 days to induce shRNA expression. Cells were treated with 10 ng/ml agrin to induce AChR clusters for 12 h. Cells were stained with 10 mg/ml Axexa594-conjugated α-bungarotoxin (1:100, Invitrogen) to label AChR and fixed in 2% paraformaldehyde. Fluorescence images were observed under an Olympus XL71 fluorescence microscope and analyzed with MetaMorph software (Molecular Devices). The lengths of AChR clusters and myotubes were defined as the longest axes of Alexa594 signals and GFP signals, respectively, in the transfected cells. AChR clusters with the axis length <4 μm were excluded from the analysis.

Luciferase assays

HEK293 cells were transfected with ATF2-Luc and phRL-TK along with the *MUSK* and *LRP4* cDNAs. Cells were cultured for 24 h in the presence or absence of agrin in the medium in a 96-well plate. Cells were lysed with the passive lysis buffer (Promega) and assayed for the luciferase activity using the Dual luciferase system (Promega). Each experiment was done in triplicate.

Biotinylation of LRP4 on plasma membrane and western blotting

HEK293 cells transfected with MuSK and LRP4 plasmids in the presence of agrin were cultured for 24 h. C2C12 myoblasts transfected with shLrp4 and human *LRP4* cDNA using NEPA21 electroporator and electroporation cuvettes (NepaGene) were cultured in a differentiation medium for 2 days in the presence of 2 μg/ml doxycycline and 10 ng/ml agrin. Efficient downregulation of Lrp4 was confirmed by quantitative RT–PCR. Cells were lysed with a buffer containing 50 mM HEPES pH 7.0, 150 mM NaCl, 10% glycerol, 1% Triton X-100, 1.5 mM $MgCl_2$, 1 mM EGTA, 100 mM NaF, 10 mM sodium pyrophosphate, 1 μg/μl aprotinin, 1 μg/μl leupeptin, 1 μg/μl pepstatin A, 1 mM PMSF, 1 mM sodium orthovanadate. Cell lysates were subjected to coimmunoprecipitation using 1 μg of anti-phosphotyrosine antibody (4G10, Upstate) attached to protein G Sepharose beads (GE Healthcare). For biotinylation of LRP4 on plasma membrane, LRP4-transfected HEK293 cells were washed twice with PBS containing 1 mM $MgCl_2$ and 0.1 mM $CaCl_2$ (PBS/CM), followed by incubation with 0.5 mg/ml sulfo-NHS-SS-biotin (Pierce) in PBS/CM at room temperature for 30 min. The cells were then washed once with PBS/CM and incubated with 10 mM monoethanolamine for quenching free biotin. The cells were harvested with RIPA buffer (Pierce) after several washing with ice-cold PBS and the cell lysates were incubated with streptavidin sepharose beads (GE healthcare) to purify cell membrane protein. Total or precipitated proteins were dissolved in 1 × laemmli buffer, separated on a 10 or 7.5% SDS–polyacrylamide gel and transferred to a polyvinylidene fluoride membrane (Immobilon-P, Millipore). Membranes were washed in Tris-buffered saline containing 0.05% Tween 20 (TBS-T) and blocked for 1 h at room temperature in TBS-T with 3% bovine serum albumin. The membranes were incubated overnight at 4°C either with the mouse monoclonal anti-Myc 9E10 (dilution 1:500, sc-40, Santa Cruz Biotechnology), anti-Flag M2 (dilution 1:4000, F1804, Sigma-Aldrich), anti-LRP4 (dilution 1:1000, ab85697, Abcam), anti-MuSK (1:500, sc-6009, Santa Cruz Biotechnology) or anti-β-actin (dilution 1:200, sc-47778, Santa Cruz Biotechnology) antibody. The membranes were washed three times for 10 min with TBS-T and incubated with secondary goat anti-mouse IgG antibody conjugated to horseradish peroxidase (HRP) (1:6000, LNA931 V/AG, GE Healthcare) for 1 h at room temperature. The blots were detected with Amersham ECL western blotting detection reagents (GE Healthcare) and quantified with the ImageJ program.

Preparation of agrin-MycAP, MuSKect-MycAP and LRP4ecd-flag proteins

Agrin-mycAP and MuSKect-mycAP in the conditioned media of transfected HEK293 cells were concentrated ~100-fold using Amicon Ultra-4 filters (Millipore). For the cell surface-binding assay, we used the concentrated conditioned media. For the plate-binding assay, we further purified agrin-mycAP and MuSKect-mycAP using the c-myc-Tagged Protein Mild Purification Kit ver. 2 (MBL). Wild-type and mutant hLRP4ecd-Flag proteins were purified with the Anti-DYKDDDDK-tag Antibody Beads (Wako) from the conditioned medium of the transfected HEK293. Purified MuSKect-mycAP and hLRP4ecd-Flag were detected by anti-myc antibody (9E10, Abcam) or anti-Flag antibody (M2, Sigma-Aldrich), respectively. We also measured concentrations of each protein by SDS–PAGE followed by protein staining with SYBRO Ruby Protein Gel Stain (Molecular Probes) using BSA as a standard.

Cell surface- and plate-binding assays

For the cell surface-binding assay, COS cells were transfected with LRP4 using FuGENE 6 (Roche). Cells were incubated 24 h with concentrated conditioned medium containing either agrin-mycAP or MuSKect-mycAP for 1.5 h at RT. Cells were washed with HABH buffer (0.5 mg/ml bovine serum albumin, 0.1% NaN_3 and 20 mM HEPES, pH 7.0, in Hank's balanced salt solution), fixed in 60% acetone for 10 min on ice followed by 4% paraformaldehyde in 20 mM HEPES (pH 7.0) in Hank's balanced salt solution for 10 min on ice. Fixed cells were washed once with 20 mM HEPES (pH 7.0) and 150 mM NaCl, incubated at 65°C for 30 min, washed with 0.1 M Tris–HCl (pH 8.0), washed with water and stained with NBP/BCIP solution (Roche). For plate-biding assay, the Immuno plate (Nunc) was coated with 0.15 μg of purified wild-type or mutant LRP4ecd-Flag at 4°C overnight and then incubated with a blocking buffer (1%BSA in PBS) at RT for 1 h. For the binding assays, 80 μl of serially diluted agrin-mycAP or MuSKect-mycAP were added to wells that were coated with wild-type or mutant LRP4ecd-Flag in a blocking buffer. The reagents were incubated for 2 h at RT, and then washed twice with PBS. Bound AP activity was measured using LabAssay ALP (Wako).

Homology modeling

The primary sequence of the 3rd β-propeller domain of hLRP4 (accession number: AAI36669, amino acid 1048–1350) and the coordinates of crystal structure of the 1st β-propeller domain (amino acid 20–326) of human LRP6 (PDB ID: 3SOV) were loaded into the Molecular Operating Environment software (MOE, Chemical Computing Group). The primary structures of each β-propeller domain of hLRP4 and hLRP6 were sequence-aligned and manually corrected by the structure–alignment method. Molecular mechanics were calculated by an MMFF94x force field.

SUPPLEMENTARY MATERIAL

Supplementary Material is available at *HMG* online.

ACKNOWLEDGEMENTS

We thank Keiko Itano for expert technical assistance.

Conflict of Interest statement. None declared.

FUNDING

This work was supported by Grants-in-Aid from the MEXT and MHLW of Japan to B.O., M.I., A.M. and K.O.; and by NIH Research Grant NS6277 from the NINDS and by Research Grant from the MDA to A.G.E.

REFERENCES

1. Engel, A.G. (2012) Current status of the congenital myasthenic syndromes. *Neuromuscul. Disord.*, **22**, 99–111.
2. Kim, N., Stiegler, A.L., Cameron, T.O., Hallock, P.T., Gomez, A.M., Huang, J.H., Hubbard, S.R., Dustin, M.L. and Burden, S.J. (2008) Lrp4 is a receptor for agrin and forms a complex with MuSK. *Cell*, **135**, 334–342.
3. Zhang, B., Luo, S., Wang, Q., Suzuki, T., Xiong, W.C. and Mei, L. (2008) LRP4 serves as a coreceptor of agrin. *Neuron*, **60**, 285–297.
4. Zhang, W., Coldefy, A.S., Hubbard, S.R. and Burden, S.J. (2011) Agrin binds to the N-terminal region of Lrp4 protein and stimulates association between Lrp4 and the first immunoglobulin-like domain in muscle-specific kinase (MuSK). *J. Biol. Chem.*, **286**, 40624–40630.
5. Wu, H., Xiong, W.C. and Mei, L. (2010) To build a synapse: signaling pathways in neuromuscular junction assembly. *Development*, **137**, 1017–1033.
6. Yumoto, N., Kim, N. and Burden, S.J. (2012) Lrp4 is a retrograde signal for presynaptic differentiation at neuromuscular synapses. *Nature*, **489**, 438–442.
7. Wu, H., Lu, Y., Shen, C., Patel, N., Gan, L., Xiong, W.C. and Mei, L. (2012) Distinct roles of muscle and motoneuron LRP4 in neuromuscular junction formation. *Neuron*, **75**, 94–107.
8. Higuchi, O., Hamuro, J., Motomura, M. and Yamanashi, Y. (2011) Autoantibodies to low-density lipoprotein receptor-related protein 4 in myasthenia gravis. *Ann. Neurol.*, **69**, 418–422.
9. Zhang, B., Tzartos, J.S., Belimezi, M., Ragheb, S., Bealmear, B., Lewis, R.A., Xiong, W.C., Lisak, R.P., Tzartos, S.J. and Mei, L. (2012) Autoantibodies to lipoprotein-related protein 4 in patients with double-seronegative myasthenia gravis. *Arch. Neurol.*, **69**, 445–451.
10. Pevzner, A., Schoser, B., Peters, K., Cosma, N.C., Karakatsani, A., Schalke, B., Melms, A. and Kroger, S. (2012) Anti-LRP4 autoantibodies in AChR- and MuSK-antibody-negative myasthenia gravis. *J. Neurol.*, **259**, 427–435.
11. Li, Y., Pawlik, B., Elcioglu, N., Aglan, M., Kayserili, H., Yigit, G., Percin, F., Goodman, F., Nurnberg, G., Cenani, A. *et al.* (2010) LRP4 mutations alter Wnt/beta-catenin signaling and cause limb and kidney malformations in Cenani–Lenz syndrome. *Am. J. Hum. Genet.*, **86**, 696–706.
12. Leupin, O., Piters, E., Halleux, C., Hu, S., Kramer, I., Morvan, F., Bouwmeester, T., Schirle, M., Bueno-Lozano, M., Fuentes, F.J. *et al.* (2011) Bone overgrowth-associated mutations in the LRP4 gene impair sclerostin facilitator function. *J. Biol. Chem.*, **286**, 19489–19500.
13. Styrkarsdottir, U., Halldorsson, B.V., Gretarsdottir, S., Gudbjartsson, D.F., Walters, G.B., Ingvarsson, T., Jonsdottir, T., Saemundsdottir, J., Snorradottir, S., Center, J.R. *et al.* (2009) New sequence variants associated with bone mineral density. *Nat. Genet.*, **41**, 15–17.
14. Choi, H.Y., Dieckmann, M., Herz, J. and Niemeier, A. (2009) Lrp4, a novel receptor for Dickkopf 1 and sclerostin, is expressed by osteoblasts and regulates bone growth and turnover in vivo. *PLoS ONE*, **4**, e7930.
15. Johnson, E.B., Steffen, D.J., Lynch, K.W. and Herz, J. (2006) Defective splicing of Megf7/Lrp4, a regulator of distal limb development, in autosomal recessive mulefoot disease. *Genomics*, **88**, 600–609.
16. Johnson, E.B., Hammer, R.E. and Herz, J. (2005) Abnormal development of the apical ectodermal ridge and polysyndactyly in Megf7-deficient mice. *Hum. Mol. Genet.*, **14**, 3523–3538.
17. Rasi, S., Spina, V., Bruscaggin, A., Vaisitti, T., Tripodo, C., Forconi, F., De Paoli, L., Fangazio, M., Sozzi, E., Cencini, E. *et al.* (2011) A variant of the LRP4 gene affects the risk of chronic lymphocytic leukaemia transformation to Richter syndrome. *Br. J. Haematol.*, **152**, 284–294.

18. Adzhubei, I.A., Schmidt, S., Peshkin, L., Ramensky, V.E., Gerasimova, A., Bork, P., Kondrashov, A.S. and Sunyaev, S.R. (2010) A method and server for predicting damaging missense mutations. *Nat. Methods*, **7**, 248–249.
19. Kumar, P., Henikoff, S. and Ng, P.C. (2009) Predicting the effects of coding non-synonymous variants on protein function using the SIFT algorithm. *Nat. Protoc.*, **4**, 1073–1081.
20. Schwarz, J.M., Rodelsperger, C., Schuelke, M. and Seelow, D. (2010) MutationTaster evaluates disease-causing potential of sequence alterations. *Nat. Methods*, **7**, 575–576.
21. Ohkawara, B. and Niehrs, C. (2011) An ATF2-based luciferase reporter to monitor non-canonical Wnt signaling in Xenopus embryos. *Dev. Dyn.*, **240**, 188–194.
22. Okada, K., Inoue, A., Okada, M., Murata, Y., Kakuta, S., Jigami, T., Kubo, S., Shiraishi, H., Eguchi, K., Motomura, M. *et al.* (2006) The muscle protein Dok-7 is essential for neuromuscular synaptogenesis. *Science*, **312**, 1802–1805.
23. Zong, Y., Zhang, B., Gu, S., Lee, K., Zhou, J., Yao, G., Figueiredo, D., Perry, K., Mei, L. and Jin, R. (2012) Structural basis of agrin-LRP4-MuSK signaling. *Genes. Dev.*, **26**, 247–258.
24. Zhou, H., Glass, D.J., Yancopoulos, G.D. and Sanes, J.R. (1999) Distinct domains of MuSK mediate its abilities to induce and to associate with postsynaptic specializations. *J. Cell Biol.*, **146**, 1133–1146.
25. Huze, C., Bauche, S., Richard, P., Chevessier, F., Goillot, E., Gaudon, K., Ben Ammar, A., Chaboud, A., Grosjean, I., Lecuyer, H.A. *et al.* (2009) Identification of an agrin mutation that causes congenital myasthenia and affects synapse function. *Am. J. Hum. Genet.*, **85**, 155–167.
26. Chevessier, F., Faraut, B., Ravel-Chapuis, A., Richard, P., Gaudon, K., Bauche, S., Prioleau, C., Herbst, R., Goillot, E., Ioos, C. *et al.* (2004) MUSK, a new target for mutations causing congenital myasthenic syndrome. *Hum. Mol. Genet.*, **13**, 3229–3240.
27. Selcen, D., Fukuda, T., Shen, X.-M. and Engel, A.G. (2004) Are MuSK antibodies the primary cause of myasthenic symptoms? *Neurology*, **62**, 1945–1950.
28. Shiraishi, H., Motomura, M., Yoshimura, T., Fukudome, T., Fukuda, T., Nakao, Y., Tsujihata, M., Vincent, A. and Eguchi, K. (2005) Acetylcholine receptors loss and postsynaptic damage in MuSK antibody-positive myasthenia gravis. *Ann. Neurol.*, **57**, 289–293.
29. Punga, A.R., Maj, M., Lin, S., Meinen, S. and Ruegg, M.A. (2011) MuSK levels differ between adult skeletal muscles and influence postsynaptic plasticity. *Eur. J. Neurosci.*, **33**, 890–898.
30. Bao, J., Zheng, J.J. and Wu, D. (2012) The structural basis of DKK-mediated inhibition of Wnt/LRP signaling. *Sci. Signal*, **5**, pe22.
31. Karner, C.M., Dietrich, M.F., Johnson, E.B., Kappesser, N., Tennert, C., Percin, F., Wollnik, B., Carroll, T.J. and Herz, J. (2010) Lrp4 regulates initiation of ureteric budding and is crucial for kidney formation–a mouse model for Cenani-Lenz syndrome. *PLoS ONE*, **5**, e10418.
32. Glinka, A., Wu, W., Delius, H., Monaghan, A.P., Blumenstock, C. and Niehrs, C. (1998) Dickkopf-1 is a member of a new family of secreted proteins and functions in head induction. *Nature*, **391**, 357–362.
33. Semenov, M., Tamai, K. and He, X. (2005) SOST is a ligand for LRP5/LRP6 and a Wnt signaling inhibitor. *J. Biol. Chem.*, **280**, 26770–26775.
34. Lu, Y., Tian, Q.B., Endo, S. and Suzuki, T. (2007) A role for LRP4 in neuronal cell viability is related to apoE-binding. *Brain Res.*, **1177**, 19–28.
35. Ohazama, A., Johnson, E.B., Ota, M.S., Choi, H.Y., Porntaveetus, T., Oommen, S., Itoh, N., Eto, K., Gritli-Linde, A., Herz, J. *et al.* (2008) Lrp4 modulates extracellular integration of cell signaling pathways in development. *PLoS ONE*, **3**, e4092.
36. Fambrough, D.M., Engel, A.G. and Rosenberry, T.L. (1982) Acetylcholinesterase of human erythrocytes and neuromuscular junctions: homologies revealed by monoclonal antibodies. *Proc. Natl. Acad. Sci. USA*, **79**, 1078–1082.
37. Gautron, J. (1974) Cytochimie ultrastructurale des acétylcholinestérases. *Microscopie*, **21**, 259–264.
38. Engel, A.G. (2004) In Engel, A.G. and Franzini-Armstrong, C. (eds.), *Myology*. 3rd edn. McGraw Hill, New York, Vol. I, pp. 681–690.
39. Engel, A.G. (1994) In Engel, A.G. and Franzini-Armstrong, C. (eds.), *Myology*. 2nd edn. McGraw-Hill, New York, Vol. 2, pp. 1018–1045.
40. Engel, A.G., Lindstrom, J.M., Lambert, E.H. and Lennon, V.A. (1977) Ultrastructural localization of the acetylcholine receptor in myasthenia gravis and in its experimental autoimmune model. *Neurology*, **27**, 307–315.
41. Engel, A.G., Nagel, A., Walls, T.J., Harper, C.M. and Waisburg, H.A. (1993) Congenital myasthenic syndromes: I. Deficiency and short open-time of the acetylcholine receptor. *Muscle Nerve*, **16**, 1284–1292.
42. Uchitel, O., Engel, A.G., Walls, T.J., Nagel, A., Atassi, M.Z. and Bril, V. (1993) Congenital myasthenic syndromes: II. Syndrome attributed to abnormal interaction of acetylcholine with its receptor. *Muscle Nerve*, **16**, 1293–1301.
43. Milone, M., Hutchinson, D.O. and Engel, A.G. (1994) Patch-clamp analysis of the properties of acetylcholine receptor channels at the normal human endplate. *Muscle Nerve*, **17**, 1364–1369.
44. Shen, X.M., Brengman, J.M., Sine, S.M. and Engel, A.G. (2012) Myasthenic syndrome AChRalpha C-loop mutant disrupts initiation of channel gating. *J. Clin. Invest.*, **122**, 2613–2621.